

# Interweaving Chiral Spirals

Toru Kojo <sup>a</sup>, Yoshimasa Hidaka <sup>b</sup>, Kenji Fukushima <sup>c</sup>,  
 Larry D. McLerran <sup>a,d</sup>, Robert D. Pisarski <sup>d</sup>

<sup>a</sup>*RIKEN BNL Research Center, Brookhaven National Laboratory, Upton,  
 NY-11973, USA*

<sup>b</sup>*Mathematical Physics Laboratory, RIKEN Nishina Center, Saitama 351-0198,  
 Japan*

<sup>c</sup>*Department of Physics, Keio University, Kanagawa 223-8522, Japan*

<sup>d</sup>*Department of Physics, Brookhaven National Laboratory, Upton, NY-11973,  
 USA*

---

## Abstract

We elaborate how to construct interweaving chiral spirals in (2+1) dimensions, defined as a superposition of chiral spirals oriented in different directions. We divide a two-dimensional Fermi sea into distinct wedges, characterized by the opening angle  $2\Theta$  and depth  $Q \simeq p_F$ , where  $p_F$  is the Fermi momentum. In each wedge, the energy is lowered by forming a single chiral spiral. The optimal values for  $\Theta$  and  $Q$  are chosen by balancing this gain in energy versus the cost of deforming the Fermi surface (which dominates at large  $\Theta$ ) and patch-patch interactions (dominant at small  $\Theta$ ). Using a non-local four-Fermi interaction model, we estimate the gain and cost in energy by expanding in terms of  $1/N_c$  (where  $N_c$  is the number of colors),  $\Lambda_{\text{QCD}}/Q$ , and  $\Theta$ . Due to a form factor in our non-local model, at small  $1/N_c$  the mass gap (chiral condensate) is large, and the interaction among quarks and the condensate *local* in momentum space. Consequently, interactions between different patches are localized near their boundaries, and it is simple to embed many chiral spirals. We identify the dominant and subdominant terms at high density and categorize formulate an expansion in terms of  $\Lambda_{\text{QCD}}/Q$  or  $\Theta$ . The kinetic term in the transverse directions is subdominant, so that techniques from (1+1)-dimensional systems can be utilized. To leading order in  $1/N_c$  and  $\Lambda_{\text{QCD}}/Q$ , the total gain in energy is  $\sim p_F \Lambda_{\text{QCD}}^2$  with  $\Theta \sim (\Lambda_{\text{QCD}}/p_F)^{3/5}$ . Since  $\Theta$  decreases with increasing  $p_F$ , there should be phase transitions associated with the change in the wedge number. We also argue the effects of subdominant terms at lower density where the large- $N_c$  approximation is more reliable.

---

# 1 Introduction and Our Central Results

In recent works [1,2,3,4,5,6], it has been argued that there is a new state of QCD, Quarkyonic matter, at high baryon density and low to intermediate temperatures.

This novel state exists at densities large compared to the QCD scale, so that the Fermi sea is best thought of in terms of quark degrees of freedom; it is, nevertheless, confining. It may be thought of as a Fermi sea of approximately free quarks, but with thermal and Fermi surface excitations made of color-confined mesons and baryons. The name “Quarkyonic” expresses this dualism.

While the arguments for the existence of Quarkyonic matter are rigorous only in the limit of large number of colors, for three colors this may not be such a bad approximation, at least for some range of density. The inter-quark potential inferred from the charmonium spectrum is linear out to distances of  $\sim$  fm, indicating that the production of quark anti-quark pairs is not very efficient in tempering its growth. One way of understanding is the large- $N_c$  limit where quark pairs are suppressed by  $1/N_c$  [7]. Similarly, in numerical studies of lattice QCD, the (pseudo-)critical temperature of the phase transition is a slowly varying function of baryon density, certainly for small density [8].

At high baryon density, one might expect that chiral symmetry is restored while quark confinement survives. In fact for a spatially homogeneous chiral condensate, several computations have confirmed this expectation [3,4]. This conclusion was challenged by later analysis [9] and by simple phenomenological arguments which suggest that chiral symmetry is broken in a confining phase of QCD [10].

For a spatially homogeneous phase, the restoration of chiral symmetry is understood as follows. In a homogenous phase, the scalar mesons that condense to form the chiral condensate have zero net momentum. Usually a chiral condensate, composed of quarks and anti-quarks, is not energetically favored, since popping an anti-quark up from the Dirac sea, to above the Fermi sea, costs  $\mu_q \simeq p_F$ , where  $\mu_q$  is the quark chemical potential, and  $p_F$  the quark Fermi momentum. Another way of forming a homogeneous chiral condensate is to pair up quarks with quark-holes near the Fermi surface; see the left panel in Fig. 1. In the presence of a Fermi sea, to make a scalar with zero net momentum one pairs a quark with momentum  $\vec{p}_F$  with a quark hole with momentum  $-\vec{p}_F$ . The relative momentum of the quark and the quark-hole is large, so that in a confining theory, the string tension of the bound requires that the excitation energy of such a bound state is of order  $2\mu_q$  relative to that of the scalar meson in vacuum<sup>1</sup>. Since it is unlikely that such highly excited

---

<sup>1</sup> Presumably this is a sufficient condition not to have homogeneous particle-hole

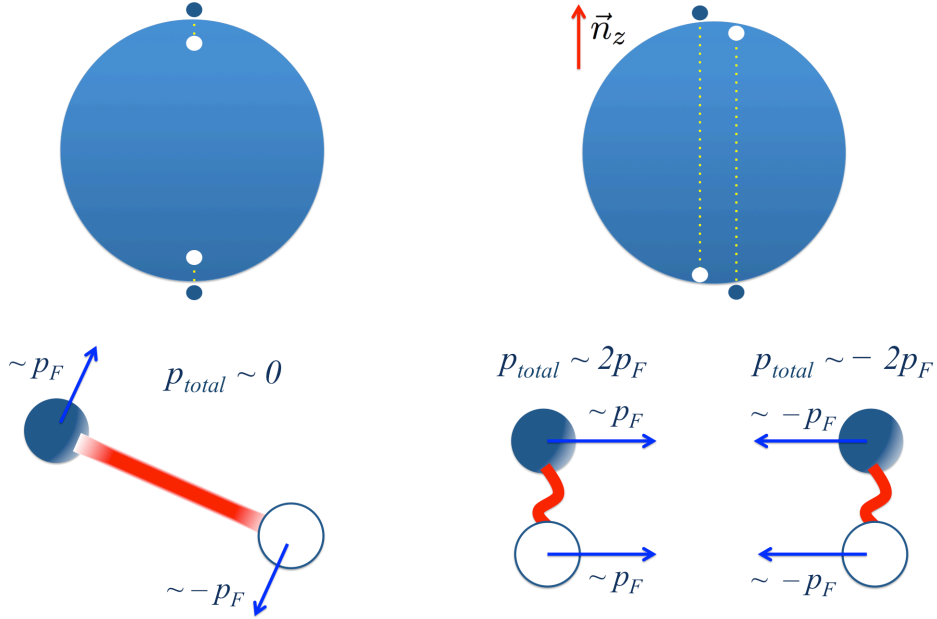


Fig. 1. Particle-hole pairing with a confining interaction. (Left): A homogeneous chiral condensate, with total momentum  $\vec{p}_{\text{total}} = \vec{0}$ . The relative momentum between a particle and a hole is large. (Right): An inhomogeneous chiral condensate with  $\vec{p}_{\text{total}} \simeq \pm 2p_F \vec{n}_z$ . The relative momentum is small. A superposition of pairs with momenta  $\vec{p}_{\text{total}} \simeq 2p_F \vec{n}_z$  and  $\vec{p}_{\text{total}} \simeq -2p_F \vec{n}_z$  creates chiral spirals.

scalar mesons condense, then chiral symmetry restoration occurs.

Another possibility is that charge density waves form through the condensation of particles and holes [11,12,13,14,15], similar to  $p$ -wave pion condensation in nuclear matter [16]. Early studies using perturbative gluon propagators [12,13] argued that the charge density waves are only realized if the number of colors is very large. These arguments, however, do not take confinement into account. More precisely, the attractive force in the infrared (IR) sector is not strong enough to overtake screening. In a recent paper [17], several of us have argued that in Quarkyonic matter, translationally non-invariant chiral condensates form as chiral spirals. The argument for a translationally non-invariant condensate follows again from a particle-hole pair near the Fermi surface; see the right panel in Fig. 1. A difference from the homogeneous condensate is that quarks and quark-holes co-move in the same spatial direction, and thereby exchange only small momenta of the order of  $\Lambda_{\text{QCD}}$ , where  $\Lambda_{\text{QCD}}$  denotes the typical scale of QCD. In contrast to the homogeneous case, the bound state which forms does not cost much energy, and condensation is possible. One finds that the optimal mode of condensation is a linear combination of the chiral condensate,  $\langle \bar{\psi}\psi \rangle$ , and an excitation which has spin-one, is an isosin-

---

condensation. Actually, even without confinement, it is likely that the condensation of chiral density waves is favored. See discussions below Eq. (44).

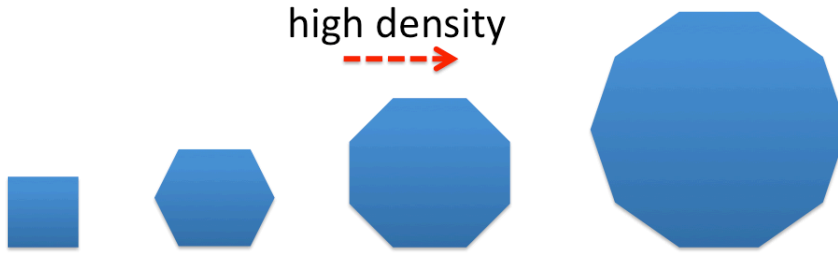


Fig. 2. The two-dimensional slice of the Fermi sea, suggested in Ref. [19]. Rotational symmetry is spontaneously broken from continuous to discrete one. The number of patches accompanying chiral spirals in different directions increases with increasing density.

glet, and has odd-parity,  $\langle \bar{\psi} \sigma^{0z} \psi \rangle$ . Here  $z$  is the direction of motion of the wave [12,17], and we call the “longitudinal” direction; those directions orthogonal to  $z$  are the “transverse” directions. The chiral spiral is characterized by a spatial oscillation between these two modes. This combination can be naturally interpreted as a superposition of particle-hole condensates with momenta  $\sim \pm 2p_F \vec{n}_z$ . At high density, like heavy-quark symmetry, there emerges an approximate symmetry of  $SU(2N_f)_+ \times SU(2N_f)_-$  [12], where  $\pm$  expresses (1+1)-dimensional chirality that characterizes the moving directions along the  $z$  axis. After the formation of chiral spirals, there are  $(2N_f)^2$  Nambu-Goldstone (NG) modes:  $(2N_f)^2 - 1$  isospin-spin excitation modes and one phonon mode, associated with spontaneous breaking of spin-chiral and translational symmetry, respectively<sup>2</sup>. These results were derived by the dimensional reduction from the (3+1)-dimensional self-consistent equations to those in the (1+1)-dimensional ’t Hooft model for degrees of freedom near the Fermi surface.

The stability analysis of Ref. [17] showed that Quarkyonic matter in the absence of a chiral condensate was unstable with respect to the formation of a (1+1)-dimensional chiral spiral. Furthermore, it was suggested that many chiral spirals of different spatial orientations interweave to form a more complicated condensate [19]. This corresponds to a transition from a spherical Fermi surface into patches, inducing breaking of continuous rotational symmetry down to discrete one (see Fig. 2). The number of patches increases as the density grows up and such phase transitions continue to occur until the screening effect on gluons strongly reduces the IR attraction between a pair of a quark and a quark-hole. Such reduction happens around the density scale,  $\mu_q \sim N_c^{1/2} \Lambda_{\text{QCD}}$  [1].

<sup>2</sup> The formation of a single chiral spiral breaks rotational symmetry in addition to translational symmetry. Since the translation and rotation are not independent, only one phonon mode appears as an NG mode [18].

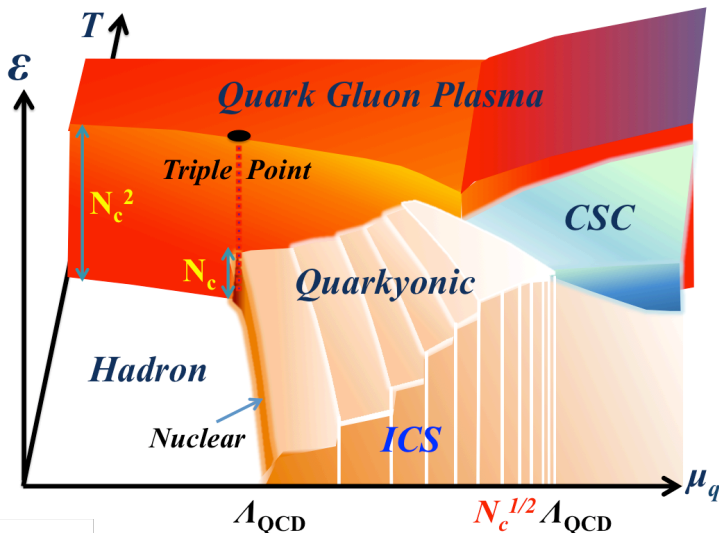


Fig. 3. The three dimensional plot of the phase diagram in  $\mu_q$ - $T$ - $\mathcal{E}$  space ( $\mathcal{E}$  is the energy density of the system). Chiral symmetry in Quarkyonic matter is broken by the formation of the interweaving chiral spirals (ICS). The stair-like growth of the energy density along  $\mu_q$  axis expresses the discontinuous change in the shape of the Fermi sea (Fig.2).

These behavior are sketched in a the phase diagram in  $\mu_q$ - $T$ - $\mathcal{E}$  space, as shown in Fig. 3 ( $\mathcal{E}$  is the energy density of the system)<sup>3</sup>. Quarkyonic matter starts to appear just above  $\mu_q \sim \Lambda_{\text{QCD}}$ , where a transition from nuclear to quark matter quickly occurs, and continues to exist up to  $\mu_q \sim N_c^{1/2} \Lambda_{\text{QCD}}$ . In the Quarkyonic region, the stair-like growth of the energy density along  $\mu_q$  axis reflects the discontinuous changes in the shape of the Fermi sea (Fig. 2). At larger  $\mu_q$ , the screening of the IR attraction reduces the size of the chiral spiral condensate, and accordingly, the interval of stair in  $\mu_q$  axis and jumps in  $\mathcal{E}$  become smaller. The shape of the Fermi sea smoothly approaches spherical one.

While Refs. [17,19] have argued for chiral spirals using the confining interactions, several aspects have not been explicitly shown due to technical difficulties and/or conceptual uncertainties in treating the deep IR structure of confining forces. On the other hand, while we postulate that the confining force could give a sufficient condition to drive chiral symmetry breaking, it is certainly not a necessary condition. The aforementioned phenomena may appear in a wider class of models that encompass chiral symmetry breaking even without confinement. Indeed, what is relevant for interweaving chiral spirals are Fermi surface effects and the IR enhancement of the interaction, but not precise knowledge about the deep IR region. Taking this viewpoint, we will characterize chiral symmetry breaking at high density by a simple, tractable

<sup>3</sup> Here we consider chiral limit for the light flavors and ignore the electroweak interactions.

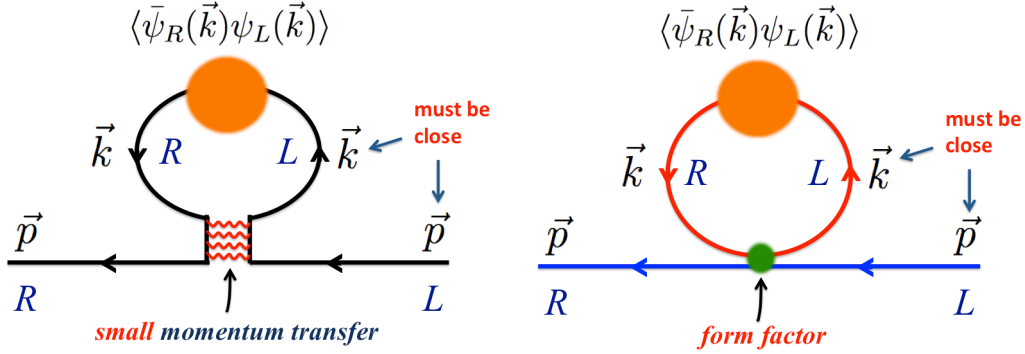


Fig. 4. The leading self-energy diagram at zero density. At large  $N_c$ , we have only to keep the rainbow ladder. (Left) The diagram in terms of QCD dynamics. Integrating the temporal component out, we can interpret the loop with momentum  $\vec{k}$  as the condensate,  $\langle \bar{\psi}(\vec{k})\psi(\vec{k}) \rangle$ , which is made of particle-antiparticle with momentum  $\vec{k}$ . (Right) The corresponding diagram in our model. The soft-gluon exchange part in QCD is replaced with the form-factor function whose strength damps as  $\vec{k}$  and  $\vec{p}$  go far apart. The diagrams for the  $1/N_c$  corrections will be given in Fig. 17 in Sec. 8.

model in which we can explore analytic insights.

We will use an effective field theory to describe QCD at large  $N_c$ . This model will be apparently similar to the Nambu–Jona-Lasinio (NJL) model [20,21] in which the dominant interacting process in the large- $N_c$  limit is the scattering of particles and the condensate. The crucial difference of our model from the usual NJL model is that the interaction vertex has a form factor that mimics the IR enhancement of the non-perturbative gluon propagator. We denote a form-factor scale of the model as  $\Lambda_f$  ( $\sim \Lambda_{\text{QCD}}$ ), beyond which interactions are negligible compared to the IR interaction.

Form-factor effects lead to the following consequences at large  $N_c$ . The interaction between a quark and a condensate becomes strongly momentum dependent; see Fig. 4. They decouple one another<sup>4</sup> if the relative momentum between the quark and the condensate is much larger than  $\Lambda_f$ , reflecting composite nature of the quark condensate. As a consequence, the quark mass gap damps when the quark momentum is far away from the domain of condensation. In vacuum, the damping scale of the mass function  $\Lambda_c$  may play a similar role to the ultraviolet (UV) cutoff,  $\Lambda_{\text{NJL}}$ , in the usual NJL model (see the left panel in Fig. 5). In this sense, the form factor can naturally remove the UV cutoff artifact of the NJL-type model.

All of these aspects are crucial when we consider dense quark matter. Since condensation phenomena should happen near the Fermi surface, the effective UV cutoff should appear in the distance from the Fermi surface, not that from

<sup>4</sup> This sort of picture has been discussed for the high-lying mesons and baryons [22]. See also Ref. [23] for some caveats on this picture.

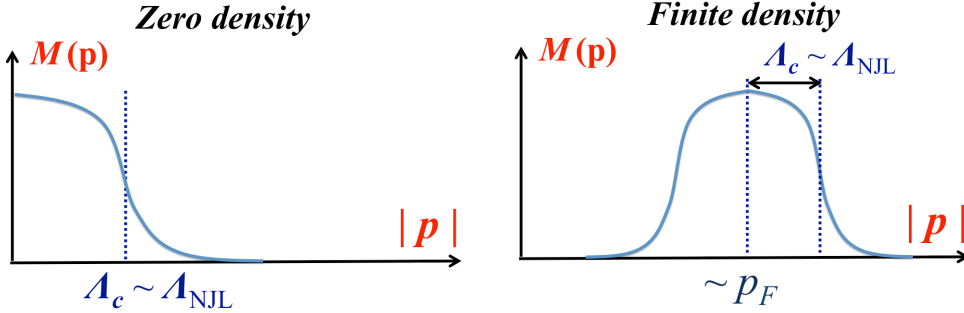


Fig. 5. Schematic figures for the mass gap function. (Left) The zero density case. (Right) The finite-density case with chiral symmetry breaking near the Fermi surface.

vacuum (see the right panel in Fig. 5). If we fixed the effective UV cutoff to be the same as the vacuum value by hand, arguments on chiral symmetry breaking would not make sense for  $\mu_q \geq \Lambda_{\text{NJL}}$ . Indeed, because of Pauli blocking, phase space for quarks contributing to the condensate would disappear, leading to chiral symmetry restoration as a cutoff artifact. Therefore it would be desirable to derive an effective UV cutoff dynamically for each density. We claim that the introduction of the form factor gives a natural extension of the treatment of the zero-density NJL model to that at finite density. Also we make a remark that the so-called Debye cutoff frequency is introduced in this way from the Fermi surface in the standard BCS theory.

With this modified NJL model at hand, the purpose of this paper is to give detailed and analytic insights on the interweaving of chiral spirals and on the associated breakdown of the rotational invariance. A key observation in our model treatment with a form factor will be that at large  $N_c$ , the particle-condensate interaction (i.e. the interaction of particles scattering off the condensate) happens *locally in momentum space*<sup>5</sup>, which will allow the system to simultaneously embed many chiral spirals at sufficiently high density.

For the sake of simplicity, we will work in (2+1) dimensions, where the original Fermi surface is a circle and takes a simple geometric structure even after formation of many chiral spirals. An extension of this study to higher dimensions might be technically difficult but conceptually straightforward.

Speaking precisely, in three space-time dimensions there is no true chiral symmetry, since there is no  $\gamma_5$  matrix for two component spinors. Using four component spinors, there is flavor symmetry breaking. This technicality does not change any of our main considerations. (Further discussions is given in Sec.2.3.)

<sup>5</sup> The  $1/N_c$  corrections (as shown in Fig. 17) will violate this locality; see discussions in Sec. 8.

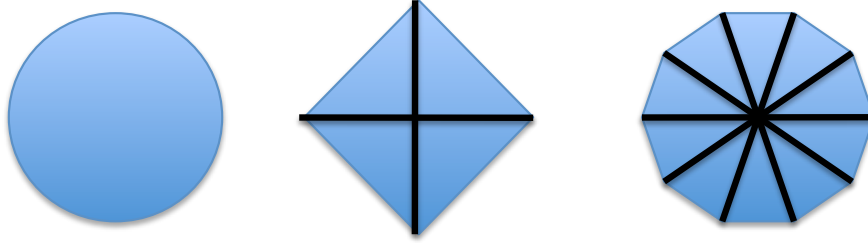


Fig. 6. The leftmost is the Fermi circle in spatial two dimensions. The middle figure is a square approximation to the circle. The wedges are shown corresponding to discrete sub-area of the circle. The rightmost figure is a higher-order polygon approximation to the circle.

We approximate the patched Fermi surface by a polygon of degree  $N_p$ . In Fig. 6 we show the two-dimensional Fermi surface and some polygon approximations to it. We will look for an energy minimum at a non-zero value of  $N_p$ , and we will find that there exists such a minimum that depends upon density. We can think of each sub-sector that constitutes the polygon shape as a wedge. The wedge is characterized by an opening angle  $2\Theta$  and a depth  $Q$  as shown in Fig. 7. The depth  $Q$  will be of the order of the Fermi momentum  $p_F$ , and the opening angle of the wedge is constrained<sup>6</sup> by  $2 \times 2N_p\Theta = 2\pi$ . The surface thickness  $\Lambda_{\text{Fermi}}$  ( $\sim \Lambda_f$ ) characterizes the momentum scale for which non-perturbative Fermi surface effects are important.

The use of the wedge shape is motivated by the following reasons: In order to maximize the energy gain from condensation effects, each patch should contain only one chiral spiral by aligning total momenta of a bunch of particle-hole pairs. If we had a misalignment, interplay among chiral spirals would reduce the size of the gap, as exemplified in Sec. 7.3. So we have to look for the most effective shape to achieve the alignment of total momenta. An obvious candidate is the flat Fermi surface with which particles and holes participating in the condensate can stay close to the Fermi surface, saving the virtual excitation energies. Other shapes require some of particles and holes with larger excitation energies, so are not effective to create a bigger condensate.

What is the principle to determine the number of patches? It is essentially determined by the balance between the kinetic-energy cost and the condensation-energy gain. Without condensation effects, the Fermi surface would simply take a circle shape that minimizes the kinetic energy. Once condensation effects are turned on, the associated energy gain can overtake the kinetic-energy cost, changing the shape of the Fermi sea from a circle to a polygon with dis-

<sup>6</sup> Here a factor 2 is included since we will take one patch as a set of one wedge and the other wedge in the opposite side of the Fermi sea. See Sec. 3 for details.



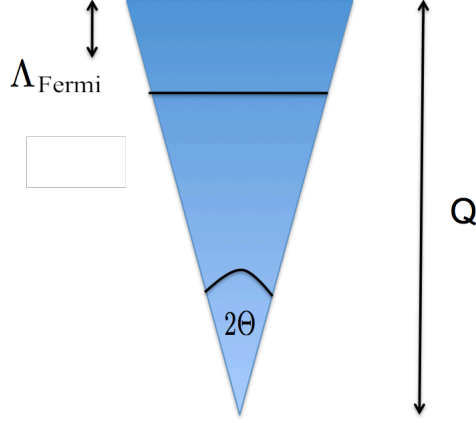


Fig. 7. The basic wedge from which the polygon is constructed. The wedge has an opening angle  $2\Theta$ , a depth  $Q$ , and a surface thickness  $\Lambda_{\text{Fermi}}$ .

create number of wedges. The condensation effects appear in two places. One is the energy reduction of single-particle contributions inside of one wedge, as is the case in the single chiral spiral problem. The other is the inter-patch interactions among different chiral spirals. The latter will provide an energy cost, that is, chiral spirals destroy one another if their wavevectors are different (as explained in Sec. 7, and also some results from the existing literatures will be addressed in Sec. 8.1). This means that we should divide the Fermi sea into not too many wedges to get the largest energy gain. Therefore the size of one wedge tends to be as large as possible until the kinetic-energy cost becomes too big.

Let us outline how to optimize the shape of the Fermi sea. In the following, we will consider the canonical ensemble, in which the particle number is fixed. Then the Fermi volume must be conserved, so it follows that

$$p_{\text{F}}^2 \Theta = Q^2 \tan \Theta. \quad (1)$$

Here the LHS is a fermion number for the plain circle shape of the Fermi sea, while the RHS is for the deformed Fermi sea. For small  $\Theta$  we can approximate the RHS by the Taylor expansion in terms of  $\Theta$ , with which we can solve  $Q(\Theta)$  as

$$Q(\Theta) = p_{\text{F}} \left( 1 - \frac{\Theta^2}{6} - \frac{\Theta^4}{40} + \dots \right). \quad (2)$$

Thus, the size of one patch in the transverse direction is

$$(\text{one patch size}) = Q(\Theta) \tan \Theta = p_{\text{F}} \Theta \left( 1 + \frac{1}{6} \Theta^2 + \frac{19}{360} \Theta^4 + \dots \right). \quad (3)$$

Now that  $Q$  is solved as a function of  $\Theta$ , the multiple chiral spiral states are characterized by  $p_{\text{F}}$ ,  $\Theta$ , and the single-particle mass gap,  $M$ . We will perform

the energy minimization by taking  $\Theta$  and  $M$  as variational parameters.

Provided that the energy minimum exists for  $\Theta \ll 1$ , we can expand the energy density by powers of  $\Theta$ . It will turn out that the expression takes the following form,

$$\begin{aligned} \mathcal{E}(M, \Theta) &= N_p \cdot \mathcal{E}^{\text{1-patch}}(M, \Theta) \\ &= \frac{\mathcal{E}_{-1}(M)}{\Theta} + \mathcal{E}_0(M) + \mathcal{E}_2(M)\Theta^2 + \mathcal{E}_4(M)\Theta^4 + \dots \end{aligned} \quad (4)$$

The  $1/\Theta$  term can appear simply because  $N_p = \pi/2\Theta$ , but it will disappear for vanishing  $M$ , that is,  $\mathcal{E}_{-1}(M \rightarrow 0) = 0$ . Expanding  $\mathcal{E}_n(M)$  by powers of  $M/p_F$ , we expect

$$\mathcal{E}_n(M) = c_n^{(0)} p_F^3 + c_n^{(1)} p_F^2 M + c_n^{(2)} p_F M^2 + \dots, \quad (5)$$

where we did not write possible non-analytic terms explicitly. (In what follows, solving the gap equation, in fact, we can arrive at the above form of the expression.) At sufficiently high density, one has only to keep the leading term in the  $M/p_F$ -expansion for each  $\mathcal{E}_n(M)$ .

Let us first discuss terms insensitive to details of condensation effects, computing at  $M = 0$ . The first non-vanishing contribution of  $O(p_F^3)$  with non-trivial  $\Theta$  dependence should arise from the kinetic-energy cost for the deformation of the Fermi surface. The energy at  $M = 0$  is an increasing function of  $\Theta$ ,

$$\begin{aligned} \mathcal{E}(M = 0, \Theta) &= N_p \cdot 2N_c \cdot 4 \int_0^Q \frac{dp_{\parallel}}{2\pi} \int_0^{p_{\parallel} \tan \Theta} \frac{dp_{\perp}}{2\pi} \sqrt{p_{\parallel}^2 + p_{\perp}^2} \\ &= N_c \cdot \frac{p_F^3}{3\pi} \left( 1 + \frac{1}{30} \Theta^4 + O(\Theta^6) \right), \end{aligned} \quad (6)$$

where the first term gives the trivial contribution which should be subtracted out<sup>7</sup>. It is extremely important to notice that the non-trivial deformation energy does not appear until  $O(\Theta^4)$ . The volume conservation of the Fermi sea cancels the  $\Theta^2$ -term out from the average kinetic energy.

Terms beyond  $O(\Theta^4)$  are much smaller than  $p_F^3 \Theta^4$  and irrelevant in our minimization procedure. Thus, the energy minimum will be found by balancing the  $p_F^3 \Theta^4$  term with condensation effects which yield terms with smaller powers of  $\Theta$  than the  $p_F^3 \Theta^4$  term. In the following we concentrate on the estimation of such condensation terms.

The condensation effects depend on interaction properties of models. The point of our model is that at large  $N_c$  the single-particle dispersion of a fermion with

<sup>7</sup> In the first line of the equation, the factor  $2N_c$  is for degeneracy factors of colors and spins for four component spinors. The second factor 4 arises because one patch is made of two opposite wedges and the  $p_{\perp}$  integral with the opening angle is  $2\Theta$ .

momentum  $\vec{p}$  is determined only by condensates within the domain of the size  $\sim \Lambda_f^2$  around  $\vec{p}$ . It means that if we consider the gap for single particles farther from patch boundaries than  $\Lambda_f$ , it will be affected only by the single chiral spiral, not by adjacent chiral spirals.

The above argument suggests that we have to evaluate the mass gap differently depending on the different domains of  $\Theta$ . then there are intersection points of more than one patch that have interactions among them. To solve the gap equation, hence, we have to take into account the influence of several chiral spirals simultaneously. This is a rather technically complicated problem. Fortunately, the energy minimum in our problem will be outside of this  $\Theta$  domain.

We can self-consistently show that the transverse size of one patch is much larger than  $\Lambda_f$ , i.e.

$$p_F \Theta \gg \Lambda_f. \quad (7)$$

Once this condition is satisfied, the single-particle gap in one patch can be determined independently from  $\Theta$ , except in the region close to the patch boundaries. We denote such a solution as  $M = M_0 \sim \Lambda_f$ . Then the energy gain from condensation effects should be

$$(\text{energy gain}) \sim N_p \cdot N_c (\Lambda_f p_F \tan \Theta) M_0 \sim N_c M_0 \Lambda_f p_F \left( 1 + \frac{\Theta^2}{3} + \dots \right), \quad (8)$$

where  $\Lambda_f p_F \tan \Theta$  is the one-patch phase space where the condensation occurs. One important observation here is that, while the gap is insensitive to  $\Theta$ , the phase space has  $\Theta$  dependence, so that the leading term is  $\Theta$  independent after multiplying a patch number  $N_p$ .

Let us see contributions at the intersection point of two adjacent patches. The point is that a particle from one patch and condensates from other patches interact within a limited domain of  $\sim \Lambda_f^2$  near the intersection points. Its phase space is independent of  $\Theta$ . Therefore the contribution from the intersection points is

$$(\text{energy cost}) \sim N_p \cdot N_c \Lambda_f^2 f(M_B) \sim \frac{N_c}{\Theta} \cdot \Lambda_f^2 f(M_B), \quad (9)$$

where  $f(M_B)$  is some function of the order  $M_B \sim \Lambda_f$  with  $M_B$  be the mass gap near the boundary, and vanishes as  $M_B \rightarrow 0$ . The contribution must be an energy cost. The reason is that in Eq. (8) we overestimated the energy gain which should be reduced around the patch boundaries. The misalignment of chiral spiral wavevectors tends to destroy the different chiral spirals one another, and reduces the size of the gap at the intersection points. Diagrammatically, this contribution will appear as interactions among chiral spiral mean fields

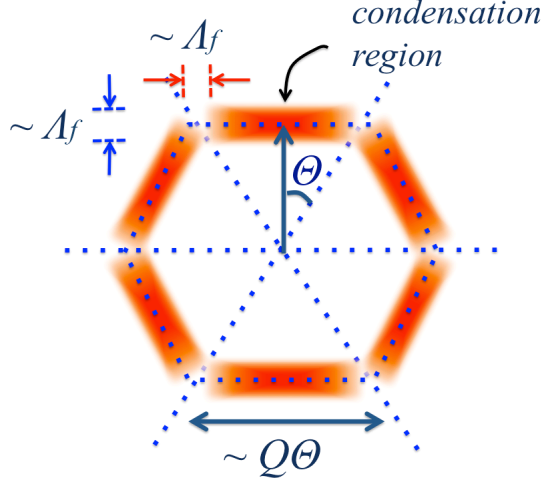


Fig. 8. The condensation region near the Fermi surface. The thickness of the region in the radial direction is  $\sim \Lambda_f$ . In the boundary region with the transverse size of  $\sim \Lambda_f$ , inter-patch interactions between the nearest-neighbor chiral spirals destroy condensates one another, reducing the energy gain from condensation effects.

in different domains. The presence of this term becomes more important for smaller  $\Theta$ .

Now we can express the energy density as a function of  $M$  and  $\Theta$ . In the domain  $\Lambda_f/p_F \ll \Theta \ll 1$ , it reads

$$\begin{aligned} \delta\mathcal{E}(M, \Theta) \\ \sim N_c \left( \frac{\Lambda_f^2 f(M_B)}{\Theta} - c_0 M_0 \Lambda_f p_F - c_2 M_0 \Lambda_f p_F \Theta^2 + c_4 p_F^3 \Theta^4 + \dots \right), \end{aligned} \quad (10)$$

where coefficients  $c_0, c_2, \dots$  are positive, and we have subtracted the free Fermi gas contribution. The energy balance is schematically illustrated in Fig. 9. To assure this expression by microscopic calculations is our goal in later sections.

When  $\Lambda_f/p_F < (\Lambda_f/p_F)^{1/2} < \Theta \ll 1$  is satisfied, the  $p_F^3 \Theta^4$  term dominates over other terms, and the deformation energy supersedes the condensation energy. Thus, there is an upper bound of  $\Theta$ , and the energy minimum should lie in the region,  $\Lambda_f/p_F \ll \Theta \ll (\Lambda_f/p_F)^{1/2}$ . On the other hand, the lower bound of  $\Theta$  will be set by the patch-patch interactions proportional to  $1/\Theta$ . In the region of current concern, we have

$$\left. \frac{\partial \delta\mathcal{E}(M, \Theta)}{\partial \Theta} \right|_{\Theta=\Theta_0} \sim N_c \left( -\frac{\Lambda_f^3}{\Theta_0^2} + 4c_4 p_F^4 \Theta_0^3 \right) \sim 0, \quad (11)$$

for the energy minimum neglecting other terms. Therefore we find

$$\Theta_0 \sim \left( \frac{\Lambda_f}{p_F} \right)^{3/5}. \quad (12)$$

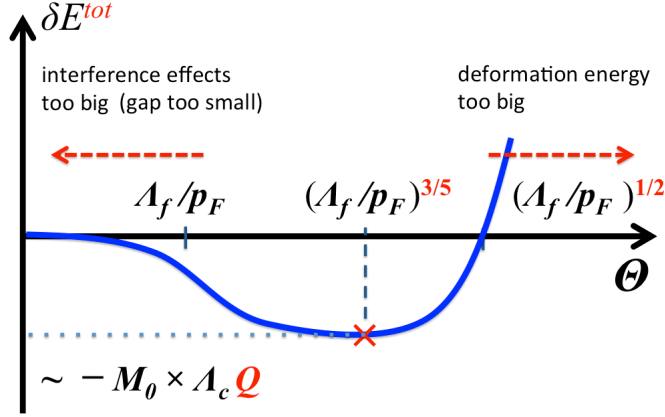


Fig. 9. The schematic energy landscape as a function of  $\Theta$ . The region  $\Theta \ll \Lambda_f/p_F$  is beyond the applicability of our analysis.

As we promised, we can confirm in this way that  $p_F \Theta_0 \sim (p_F/\Lambda_f)^{2/5} \Lambda_f \gg \Lambda_f$ , which surely justifies Eq. (7) *posteriori*.

The total energy is dominated by the condensation term  $\sim -p_F \Lambda_f^2$ , which is independent of  $\Theta_0$ . The leading corrections come from the  $1/\Theta_0$  term (patch-patch interactions) and the  $\Theta_0^4$  term (the deformation energy) which are suppressed by  $(\Lambda_f/p_F)^{2/5}$  compared to the leading contribution. This implies that after solving the one-patch problem at the mean-field level, other patch-patch contributions can be treated within perturbation theory. We will formulate our perturbation theory within the domain of  $(\Lambda_f/p_F) \ll \Theta \ll (\Lambda_f/p_F)^{1/2}$ .

This paper is organized as follows. In Sec. 2, we define our model and describe consequences of form-factor effects in vacuum. In Sec. 3, the Fermi sea is decomposed into several segments. We formally separate the Lagrangian into the one-patch and the patch-patch interactions. In Sec. 4, the mean-field treatment for the one-patch problem is discussed. We first identify the dominant terms within one patch, and construct the mean field for chiral spirals as well as the mean-field propagators for quasi-particles. In Sec. 5, we give a formal expression of the perturbative expansion. In Sec. 6, we treat corrections from subdominant terms in one patch. It will be shown that subdominant terms are suppressed by powers of  $\Theta$  or  $\Lambda_f/Q$ . In Sec. 7, the inter-patch interactions at the patch boundaries are discussed. The size and sign of  $1/\Theta$  terms are estimated in both perturbative and non-perturbative manners. In Sec. 8, we argue possible impacts of several corrections ignored in this paper. We also review other works and attempt to place this work in perspective. A coordinate space structure of the interweaving chiral spirals is also discussed, leaving several interesting questions open. Section 9 is devoted to a summary and possible future directions.

## 2 A Model: The Four-Fermi Interaction with Form-factor Effects

In this section, we introduce explicit form factors into the NJL model, so that the interaction is cutoff when the momentum transfer becomes large. This makes the NJL model non-local. (For other attempts to introduce non-locality which emphasize different aspects from ours, see Ref. [24].) We will see that effects of such a cutoff determine the momentum domains where condensation phenomena are relevant. This aspect is particularly important when we consider the very large Fermi sea in which condensation phenomena occur as Fermi surface effects, rather than the vacuum effects.

### 2.1 Form factor effects

Let us consider the scalar-scalar type of the four-Fermi interaction,

$$\int d^3x (\bar{\psi}\psi(x))^2 = \int dx_0 \int_{q,p,k} (\bar{\psi}(\vec{p} + \vec{q})\psi(\vec{p})) (\bar{\psi}(\vec{k})\psi(\vec{k} + \vec{q})), \quad (13)$$

where we define a shorthand notation,

$$\int_{q,p,k} \equiv \int \frac{d\vec{q} d\vec{p} d\vec{k}}{(2\pi)^6}, \quad (14)$$

and we did not explicitly write the coupling constant and  $x_0$  dependence of fermion fields. Since the four-Fermi interaction is not renormalizable beyond (1+1) dimensions, we need introduce some UV cutoff.

We regularize the UV interaction by including form-factor effects,

$$\int d^3x (\bar{\psi}\psi(x))^2 \rightarrow \int dx_0 \int_{q,p,k} (\bar{\psi}(\vec{p} + \vec{q})\psi(\vec{p})) (\bar{\psi}(\vec{k})\psi(\vec{k} + \vec{q})) \theta_{p,k}, \quad (15)$$

where

$$\theta_{p,k} \equiv \theta(\Lambda_f^2 - (\vec{p} - \vec{k})^2). \quad (16)$$

This mimics the form-factor effects in large- $N_c$  QCD<sup>8</sup>, and removes the UV divergences associated with interacting processes.

<sup>8</sup> Here we put the cutoff on the spatial-momentum  $\vec{p}^2$ , not on the Euclidean momentum  $p_E^2$ . So, results in this work are connected to those of large- $N_c$  QCD in the Coulomb gauge, in which the dominant non-perturbative part is of the instantaneous type [25]. An alternative choice would be to introduce a cutoff on  $p_E^2$  keeping manifest Lorentz invariance. Such a treatment should mimic, for instance, Landau-gauge results in Euclidean space. However we do not know their Minkowskian behavior, so we have to compute quantities in Euclidean space. Then the price we have to

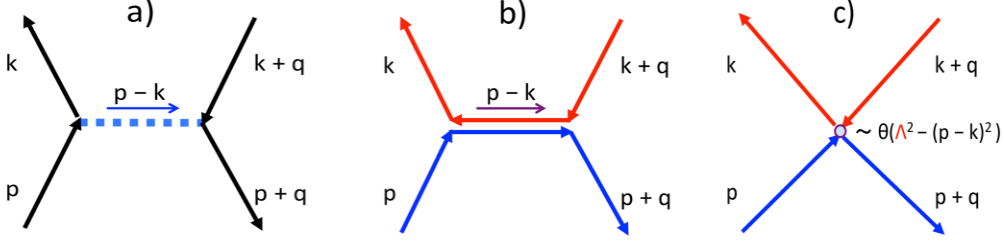


Fig. 10. (a) The non-perturbative gluon exchange which is supposed to damp quickly in the UV region. (b) The color line representation of the one-gluon exchange. (c) Our effective four-Fermi interaction including form factor effects.

The large- $N_c$  QCD is mimicked as follows. The one-gluon exchange including non-perturbative effects are shown in Fig. 10(a). Its strength damps as the momentum transfer becomes large. We roughly take into account this property by introducing a step function,  $\theta(\Lambda_f^2 - (\vec{p} - \vec{k})^2)$ , keeping the interaction strength constant. In QCD, the cutoff scale  $\Lambda_f$  should be taken to be of the order of  $\Lambda_{\text{QCD}}$ .

In Fig. 10(b), we show the color line representation to illustrate how the one-gluon exchange interaction should be contracted into a four-Fermi type interaction. Taking into account features in Figs. 10(a) and 10(b), we arrive at a simple model described in Eq. (15) and Fig. 10(c).

A relevant consequence of our choice of the form factor is that the coupling between fermion fields and the condensate becomes strongly momentum dependent. In particular, fermions decouple from the condensation effects if they belong to domains with a momentum difference of the order of  $\Lambda_f$ .

Let us first see this property in the vacuum case by investigating the Schwinger-Dyson equation for quasi-particles. After picking up the pole, we have<sup>9</sup>

$$\Sigma_m(\vec{p}) = \int \frac{d\vec{k}}{(2\pi)^2} \frac{\Sigma_m(\vec{k})}{2\epsilon(\vec{k})} \theta_{p,k}, \quad (17)$$

where  $\Sigma_m(\vec{k})$  is the self-energy and  $\epsilon(\vec{k}) = \sqrt{\vec{k}^2 + \Sigma_m^2(\vec{k})}$  is the quasi-particle energy. For its diagrammatic expression, see Fig. 4<sup>10</sup>. When  $|\vec{p}|$  is very large,  $|\vec{k}|$  must be as large because of the form factor. In the asymptotic region

pay is that a simple physical intuition does not necessarily work, especially at finite density.

<sup>9</sup> We ignored the Lorentz vector self-energy for the sake of simplicity. This simplification should not alter our basic statements in this paper.

<sup>10</sup> The Fock-type gluon exchange, which is dominant in large- $N_c$  QCD, corresponds to the Hartree term of the four-Fermi interaction model, so we can apply most of techniques used in the NJL model calculations.

$|\vec{p}| \gg \Sigma(\vec{p})$ , the Schwinger-Dyson equation looks like

$$\Sigma_m(\vec{p}) \sim \frac{1}{2\epsilon(\vec{p})} \int \frac{d\vec{k}}{(2\pi)^2} \Sigma_m(\vec{k}) \theta_{p,k}, \quad (18)$$

from which one can show that  $\Sigma_m(\vec{p})$  damps faster than  $1/\epsilon(\vec{p}) \sim 1/|\vec{p}|$  in the UV region, meaning that the scattering between quasi-particles and the mean-field condensates diminishes for large momentum.

This UV behavior tremendously simplifies considerations on the energy benefit from condensation effects. Due to decoupling from condensation effects in the UV region, the normalized energy density, in which the energy density without condensation are subtracted out, is dominated by the IR contributions. Also, the couplings between the IR and the UV regions are allowed only in the limited region constrained by the form factor effects. Thus, we can proceed with our calculations independently from details of the UV physics.

At finite density, the same argument applies if we replace the Dirac sea with the Fermi sea, namely, the excitation energy  $\epsilon(\vec{p})$  is measured from the Fermi surface instead of the vacuum. Then it follows that dominant contributions to the condensation come from fermions near the Fermi surface rather than those near vacuum.

## 2.2 Bosonization of the Model

Following usual treatments, let us introduce the auxiliary fields and formally rewrite the action. Although this formal treatment is not mandatory, it would be practically convenient to use several relations derived in this framework.

Since our four-Fermi interaction is not of the separable type, we have to modify conventional treatments slightly as

$$- \int dx_0 \int \frac{d\vec{q}}{(2\pi)^2} \Phi(\vec{q}) \Phi(-\vec{q}) \rightarrow - \int dx_0 \int_{q,p,k} \Phi(\vec{q}; \vec{p}) \theta_{p,k} \Phi(-\vec{q}; \vec{k}). \quad (19)$$

Here we did not write  $x_0$  dependence of the auxiliary boson field,  $\Phi$ , explicitly for notational simplicity. Next we shift the boson fields to generate a four-Fermi interaction,

$$\Phi(\vec{q}; \vec{p}) \rightarrow \Phi(\vec{q}; \vec{p}) + \bar{\psi}(\vec{p} + \vec{q}) \psi(\vec{p}), \quad (20)$$

then, by adding these trivial terms in  $\Phi$ , we can eliminate the four-Fermi interactions out from the original action to obtain the Yukawa-type model.



The form of the vertex is

$$- \int dx_0 \int_{q,p,k} \Phi(\vec{q}; \vec{p}) \theta_{p,k} \bar{\psi}(\vec{k}) \psi(\vec{k} + \vec{q}). \quad (21)$$

We can obtain the gap equation from  $0 = \int \mathcal{D}\Phi \mathcal{D}\Psi \mathcal{D}\bar{\Psi} \frac{\delta}{\delta \Phi(\vec{q}; \vec{p})} e^{iS}$  and find,

$$\int \frac{d\vec{k}}{(2\pi)^2} \theta_{p,k} \left\{ \langle \Phi(-\vec{q}; \vec{k}) \rangle + \langle \bar{\psi}(\vec{k}) \psi(\vec{k} + \vec{q}) \rangle \right\} = 0. \quad (22)$$

Since the equation should hold at arbitrary  $\vec{p}$ , we conclude that  $\langle \Phi(-\vec{q}; \vec{k}) \rangle = -\langle \bar{\psi}(\vec{k}) \psi(\vec{k} + \vec{q}) \rangle$  ( $\geq 0$ ), which is independent of  $x_0$ .

The relation between the mass self-energy and  $\Phi$  can be read off from the coefficient of  $\bar{\psi}\psi$  in Eq. (21), i.e.

$$\Sigma_m(\vec{q}; \vec{k}) = \int \frac{d\vec{p}}{(2\pi)^2} \Phi(\vec{q}; \vec{p}) \theta_{p,k}. \quad (23)$$

In the stationary phase approximation of the  $\Phi$ -integral (which is rigorous in the large- $N_c$  limit), we can replace  $\Phi$  with  $\langle \Phi \rangle$ . One can check that substituting the gap equation for  $\Phi$  and taking  $\vec{q} = \vec{0}$  (for uniform condensates) reproduce the Schwinger-Dyson equation in Eq. (17).

Instead of computing self-consistent solutions precisely, let us consider what kind of Ansatz would capture basic properties of stationary solutions of  $\Phi(\vec{q}; \vec{p})$ . We will apply such arguments to more complicated case at finite density where condensation effects are important near the Fermi surface.

In the vacuum case, we already know qualitative behaviors of  $\Sigma_m(\vec{q}; \vec{p})$  at high momenta from the previous arguments. Its value damps as  $|\vec{p}| \rightarrow \infty$ , leading to damping of  $\Phi(\vec{q}; \vec{p})$ , as seen in the gap equation. If we denote the characteristic scale of damping as  $\Lambda_c$ , presumably the simplest Ansatz would be

$$\Phi(\vec{q}; \vec{p}) = \Delta \cdot \theta(\Lambda_c^2 - \vec{p}^2) \delta(\vec{q}). \quad (24)$$

See also Fig. 5. In principle, not only  $\Delta$ , but also  $\Lambda_c$  should be treated as variational parameters as functions of  $\Lambda_f$  that is an intrinsic scale in our model.

Perhaps it might be helpful to mention the relationship between this Ansatz and usual spatial-momentum cutoff scheme. In our model, conventional treatment of the NJL model is recovered by taking  $\Lambda_f \rightarrow \infty$  with  $\Lambda_c$  kept fixed to be the NJL-model cutoff  $\Lambda_{\text{NJL}} \sim 600$  MeV which semi-quantitatively describes low-energy properties of the hadron phenomenology. Such successes of the NJL model imply that once we correctly cutoff *the domain of condensation*, we should be able to express the low-energy dynamics quantitatively. In

our model, this cutoff scale should be dynamically determined by adjusting a value of  $\Lambda_f$ .

Adopting this interpretation, the effective cutoff of the NJL model should be measured from the Fermi surface, not from zero momentum, because condensation effects mainly appear near the Fermi surface. This leads to a picture such that chiral symmetry is restored deeply inside of the Fermi sea but is broken near the Fermi surface.

### 2.3 Spinor Representations in (2+1) Dimensions

In this work we discuss (2+1) dimensional theory instead of (3+1) dimensional one because considerations for shapes of the Fermi surface are much simpler. On the other hand, in (2+1) dimensions, there is no chirality in a strict sense. Although this fact does not modify our main considerations, we shall give a brief remark on this special properties in (2+1) dimensions.

A spinorial representation of the Lorentz group  $SO(2, 1)$  is provided by two component spinors, with  $2 \times 2$  representation of the Dirac algebra which is given by the Pauli matrices

$$\gamma_0 = \sigma_2, \quad \gamma_1 = i\sigma_3, \quad \gamma_2 = i\sigma_1. \quad (25)$$

There is no other  $2 \times 2$  matrix anticommuting with these  $\gamma_\mu$  so that  $\gamma_5$  can not be defined.

Therefore we use a four component spinor for which  $\gamma_5$  can be defined. To get some feeling, one can imagine that fermions in (3+1) dimensions are restricted within (2+1) dimensional space by imposing some external condition as done for the Kaluza-Klein reduction. Then the  $\gamma$  matrices for four component spinors can be taken in the same way as (3+1) dimensional  $\gamma$  matrices.

We expect that this prescription is the easiest way to directly convert our (2+1) dimensional manipulations into higher dimensional ones. For further discussions on (2+1) dimensional chirality, see Ref. [27] for instance.

## 3 Decomposition of the Lagrangian into Multiple Patch Domains

In this section, we decompose the NJL Lagrangian into different segments. For the sake of simplicity, we begin with the Lagrangian with one flavor,

$$\mathcal{L} = \bar{\psi} i \not{\partial} \psi + \frac{G}{N_c} \left( (\bar{\psi} \psi)^2 + (\bar{\psi} i \gamma_5 \psi)^2 \right), \quad (26)$$

where we explicitly factor out the  $N_c$  dependence of the interaction, so that  $G = O(N_c^0)$ . In the (2+1)-dimensional system,  $G$  is dimensionful, and we take it to be  $\sim \Lambda_f^{-1}$ . Our Lagrangian has continuous chiral symmetry,  $U(1)_L \times U(1)_R$ . In this work we ignore the  $U(1)_A$  problem that is of  $O(1/N_c)$  and thus negligible. For the moment, we will not write the form factor explicitly for notational simplicity.

We introduce the unit vectors  $\vec{n}_i$  which point to the center of the  $i$ -th patch, and the unit vector  $\vec{n}_{i\perp}$  which is orthogonal to  $\vec{n}_i$ . We project out the spatial components of vectors generically as

$$p_{i\parallel} = \vec{n}_i \cdot \vec{p}, \quad p_{i\perp} = \vec{n}_{i\perp} \cdot \vec{p}. \quad (27)$$

With this definition, fermion fields can be decomposed into  $N_p$  momentum domains,

$$\begin{aligned} \psi(x) &= \int \frac{d^3p}{(2\pi)^3} \tilde{\psi}(p) e^{-ip \cdot x} \\ &= \frac{1}{(2\pi)^3} \sum_{i=1}^{N_p} \int_{-\infty}^{\infty} dp_0 \int_{-\infty}^{\infty} dp_{i\parallel} \int_{-p_{i\parallel} \tan \Theta}^{p_{i\parallel} \tan \Theta} dp_{i\perp} \tilde{\psi}(p) e^{-ip \cdot x} \\ &\equiv \sum_{i=1}^{N_p} \psi_i(x). \end{aligned} \quad (28)$$

It is worth mentioning here that our formulation has potential relevance to analytic approaches based on the high-density effective theory [26]. A single patch includes a set of two domains with  $p_{i\parallel} > 0$  and  $p_{i\parallel} < 0$  for the positive energy states, in a similar way as the (1+1)-dimensional problem. Thus, the angle for one patch is  $2 \times 2\Theta$ , and  $\Theta$  should satisfy

$$4\Theta N_p = 2\pi. \quad (29)$$

Let us first decompose the free part of the Lagrangian. Since it is diagonal in momentum space, we have

$$\mathcal{L}^{\text{kin}} = \sum_i \bar{\psi}_i i \not{\partial} \psi_i \equiv \sum_i \mathcal{L}_i^{\text{kin}}. \quad (30)$$

The decomposition of four-Fermi interactions  $\mathcal{L}^{\text{int}}$  are much more cumbersome, since the interaction terms combine different domains. Explicitly writing, it follows

$$\begin{aligned} \mathcal{L}^{\text{int}} &= \frac{G}{N_c} \left( (\bar{\psi}\psi)^2 + (\bar{\psi} i \gamma_5 \psi)^2 \right) \\ &= \frac{G}{N_c} \sum_{i,j,k,l} \left( (\bar{\psi}_i \psi_j)(\bar{\psi}_k \psi_l) + (\bar{\psi}_i i \gamma_5 \psi_j)(\bar{\psi}_k i \gamma_5 \psi_l) \right). \end{aligned} \quad (31)$$

It can be decomposed into four types of interaction terms,

$$\begin{aligned}
\sum_i \mathcal{L}_i^{\text{int}} &= \frac{G}{N_c} \sum_i \left( (\bar{\psi}_i \psi_i)^2 + (\bar{\psi}_i i\gamma_5 \psi_i)^2 \right), \\
\sum_{i \neq j} \mathcal{L}_{i,j}^{\text{int}} &= \frac{G}{N_c} \sum_{i \neq j} \left( (\bar{\psi}_i \psi_i)(\bar{\psi}_j \psi_j) + (\bar{\psi}_i i\gamma_5 \psi_i)(\bar{\psi}_j i\gamma_5 \psi_j) \right), \\
\sum_{i,j \neq k} \mathcal{L}_{i,j,k}^{\text{int}} &= \frac{2G}{N_c} \sum_{i,j \neq k} \left( (\bar{\psi}_i \psi_i)(\bar{\psi}_j \psi_k) + (\bar{\psi}_i i\gamma_5 \psi_i)(\bar{\psi}_j i\gamma_5 \psi_k) \right), \\
\sum_{i \neq j, k \neq l} \mathcal{L}_{i,j,kl}^{\text{int}} &= \frac{G}{N_c} \sum_{i \neq j, k \neq l} \left( (\bar{\psi}_i \psi_j)(\bar{\psi}_k \psi_l) + (\bar{\psi}_i i\gamma_5 \psi_j)(\bar{\psi}_k i\gamma_5 \psi_l) \right). \quad (32)
\end{aligned}$$

Except the first line, interaction terms involve fermions belonging to different patches. Now we have the Lagrangian separated into one-patch and patch-patch interactions,  $\mathcal{L} = \sum_i \mathcal{L}_i^{\text{1-patch}} + \Delta \mathcal{L}^{\text{int}}$ , where

$$\mathcal{L}_i^{\text{1-patch}} = \mathcal{L}_i^{\text{kin}} + \mathcal{L}_i^{\text{int}}, \quad \Delta \mathcal{L}^{\text{int}} = \sum_{i \neq j} \mathcal{L}_{i,j}^{\text{int}} + \sum_{i,j \neq k} \mathcal{L}_{i,j,k}^{\text{int}} + \sum_{i \neq j, k \neq l} \mathcal{L}_{i,j,kl}^{\text{int}}. \quad (33)$$

The one-patch Lagrangian will play a dominant role for condensation effects. We will first solve the one-patch problem, and then include contributions from other patches perturbatively.

## 4 The One-Patch Problem at the Mean Field Level

In this section, we provide a formal treatment of the one-patch Lagrangian. We consider sufficiently high density for which the interaction scale  $\sim \Lambda_f$  is much larger than the transverse kinetic energy near the Fermi surface which is suppressed as  $\sim \bar{p}_\perp^2/Q$  where  $Q \sim p_F$ . Then the fermion dispersion relation is robust and does not rely on the transverse momentum; corrections from the higher spatial dimensions than the (1+1)-dimensional problem are generally suppressed by extra powers of  $1/Q$ . Therefore, the gap equation for the mean field effectively becomes (1+1) dimensional. We here analyze this quasi (1+1)-dimensional problem in detail.

We first summarize some convenient notations used in (1+1) dimensions. They are useful to identify the dominant and subdominant terms for the chiral spiral formation. Then we bosonize the dominant part of the four-Fermi interactions, and construct the mean-field Lagrangian for the chiral spirals. We prepare the mean-field propagator and write the gap equation down. The results in this section are the basis for the perturbation theory, which treats subdominant terms ignored at the mean-field level.

## 4.1 Preliminaries

In (1+1)-dimensional models, the chirality (i.e. the eigenvalue of  $\gamma_5$ ) characterizes the moving directions of particles. In higher dimensions, the corresponding  $\gamma$ -matrix is not  $\gamma_5$ , but  $\Gamma_{i5} \equiv \gamma_0 \gamma_{i\parallel}$  for particles moving to the  $x_{i\parallel}$ -direction. We define

$$\psi_{i\pm} \equiv \frac{1 \pm \Gamma_{i5}}{2} \psi_i. \quad (34)$$

This  $\Gamma_{i5}$  satisfies the following algebraic relations:

$$(\Gamma_{i5})^2 = 1, \quad \{\Gamma_{i5}, \gamma_{i0}\} = 0, \quad \{\Gamma_{i5}, \gamma_{i\parallel}\} = 0, \quad [\Gamma_{i5}, \gamma_{i\perp}] = 0. \quad (35)$$

The free Lagrangian can be decomposed into two pieces. The longitudinal part is defined with  $(+, +)$  or  $(-, -)$  combinations<sup>11</sup>;

$$\mathcal{L}_{i\parallel}^{\text{kin}} = \psi_{i+}^\dagger i(\partial_0 - \partial_{i\parallel}) \psi_{i+} + \psi_{i-}^\dagger i(\partial_0 + \partial_{i\parallel}) \psi_{i-}, \quad (36)$$

and the part made of  $(+, -)$  combinations is

$$\mathcal{L}_{i\perp}^{\text{kin}} = \bar{\psi}_{i+} i \not{\partial}_\perp \psi_{i-} + \bar{\psi}_{i-} i \not{\partial}_\perp \psi_{i+}. \quad (37)$$

Below, we will drop off the index  $i$  as far as no confusion arises.

At finite density with the Fermi momentum  $Q$ , it is natural to measure momenta of fermions from the Fermi surface. Accordingly, we take fields with shifted momenta<sup>12</sup>,

$$\psi_\pm(x) = e^{iQx_\parallel \Gamma_5} \psi'_\pm(x) = e^{\pm iQx_\parallel} \psi'_\pm(x) \quad (38)$$

or

$$\psi'_\pm(\delta\vec{p}) = \psi_\pm(\delta p_\parallel \pm Q, p_\perp), \quad (\delta\vec{p} = (\delta p_\parallel, p_\perp)), \quad (39)$$

in momentum space. We use the notation  $\delta\vec{p}$  to emphasize that momenta of  $\psi'$  field are measured from the Fermi surface. Using the  $\psi'$  field, one can easily identify dominant and subdominant terms at large density.

In the  $\psi'$ -representation, the longitudinal part becomes<sup>13</sup>

$$\mathcal{L}_{i\parallel}^{\text{kin}} \rightarrow \psi'_+{}^\dagger [i(\partial_0 - \partial_\parallel) - Q] \psi'_+ + \psi'_-{}^\dagger [i(\partial_0 + \partial_\parallel) - Q] \psi'_-, \quad (40)$$

<sup>11</sup> Our definition of  $\bar{\psi} = \psi^\dagger \gamma^0$ . Our metric is  $g_{\mu\nu} = g^{\mu\nu} = \text{diag}(1, -1, -1)$ .

<sup>12</sup> We will use lower index expressions for momenta, and  $Q$  should be interpreted as the lower component. And when we use the vector, that means the lower index components. For instance,  $\vec{q} = (q_1, q_2)$  and  $\vec{x} = (x_1, x_2)$ .

<sup>13</sup> In the grand canonical ensemble the basis  $\psi'$  with  $Q = \mu_q$  eliminates the chemical potential term reflecting that in the  $\psi'$ -representation we can deal with dynamics

and the transverse kinetic term and the mass term acquire the oscillating factors,

$$\mathcal{L}_{\perp}^{\text{kin}} \rightarrow \bar{\psi}'_+ i \not{\partial}_{\perp} \psi'_- e^{-2iQx_{\parallel}} + \bar{\psi}'_- i \not{\partial}_{\perp} \psi'_+ e^{2iQx_{\parallel}}. \quad (41)$$

Such oscillatory terms are suppressed near the Fermi surface by powers of  $1/Q$ . In the free theory, in fact, the excitation energy at  $|\delta p_{\parallel}| \ll Q$  is

$$\epsilon^{\text{free}}(\delta \vec{p}) = \sqrt{(Q + \delta p_{\parallel})^2 + p_{\perp}^2} - Q = |\delta p_{\parallel}| + \frac{\delta p_{\parallel}^2 + p_{\perp}^2}{2Q} + \dots. \quad (42)$$

Terms with oscillating factors define what we call ‘‘subdominant’’ terms.

The four-Fermi interactions can be also separated into dominant terms and subdominant terms,

$$\begin{aligned} (\bar{\psi}\psi)^2 &= \frac{1}{2} \left( (\bar{\psi}\psi)^2 + (\bar{\psi} i \Gamma_5 \psi)^2 \right) + \frac{1}{2} \left( (\bar{\psi}\psi)^2 - (\bar{\psi} i \Gamma_5 \psi)^2 \right) \\ &= 2 (\bar{\psi}_+ \psi_-) (\bar{\psi}_- \psi_+) + \left( (\bar{\psi}_- \psi_+)^2 + (\bar{\psi}_+ \psi_-)^2 \right) \\ &\longrightarrow 2 (\bar{\psi}'_+ \psi'_-) (\bar{\psi}'_- \psi'_+) + (\bar{\psi}'_- \psi'_+)^2 e^{4iQx_{\parallel}} + (\bar{\psi}'_+ \psi'_-)^2 e^{-4iQx_{\parallel}}. \end{aligned} \quad (43)$$

The first term corresponds to the continuous symmetric part, which becomes IR dominant at high density. We will apply the mean-field Ansatz to dominant terms, while subdominant terms are treated as perturbation. In this treatment, a gap will be found only near the Fermi surface. The gaps will not open periodically in momentum space because of the absence of different harmonics<sup>14</sup>.

Finally, for later convenience, we write Eq. (43) in momentum space including the form factor explicitly. For  $(+-)(-+)$  combinations of the dominant part, we have

$$\begin{aligned} &\int_{q,p,k} \left( \bar{\psi}_+(\vec{p} + \vec{q}) \psi_-(\vec{p}) \right) \left( \bar{\psi}_-(\vec{k}) \psi_+(\vec{k} + \vec{q}) \right) \theta_{p,k} \\ &= \int_{q,\delta p,\delta k} \left( \bar{\psi}'_+(\delta \vec{p} + \vec{q} - 2Q\vec{n}) \psi'_-(\delta \vec{p}) \right) \left( \bar{\psi}'_-(\delta \vec{k}) \psi'_+(\delta \vec{k} + \vec{q} - 2Q\vec{n}) \right) \theta_{\delta p,\delta k}. \end{aligned} \quad (44)$$

near the Fermi surface as in vacuum. This simple logic is not directly applicable in the canonical ensemble since the density constraint does not explicitly appear at the Lagrangian level.

<sup>14</sup> The current problem is different from the problem of the Peierls instability with an external periodic potential. In our case the coupling between the mean field and particles depend on the  $\pm$  combination. For instance, the mean field  $\langle \bar{\psi}_+ \psi_- \rangle = \Delta e^{-2iQx_{\parallel}}$  can scatter the particles from the  $+$  region to the  $-$  region, but cannot scatter from the  $-$  region to the  $+$  region. In this way particles and holes are kept around the Fermi surface, without going to the higher harmonic regions.

Note that if  $\vec{q} \simeq 2Q\vec{n}$ , all fields can be close to the Fermi surface simultaneously when  $\delta\vec{p} \sim \delta\vec{k} \sim \vec{0}$ . This is the reason why the configuration with  $\vec{q} \sim 2Q\vec{n}$  becomes dominant in the path integral. For this reason, we should choose the wave vector of the chiral spirals to be  $\vec{q} = 2Q\vec{n}$  in the high-density limit. This expression also indicates that the exciton-type condensation (i.e. homogeneous chiral condensation) with  $\vec{q} = \vec{0}$  is not favored energetically.

On the other hand, for  $(+-)(+-)$  combinations of the subdominant part, we have

$$\begin{aligned} & \int_{q,p,k} \left( \bar{\psi}_+(\vec{p} + \vec{q}) \psi_-(\vec{p}) \right) \left( \bar{\psi}_+(\vec{k}) \psi_-(\vec{k} + \vec{q}) \right) \theta_{p,k} \\ &= \int_{q,\delta p,\delta k} \left( \bar{\psi}'_+(\delta\vec{p} + \vec{q} - 2Q\vec{n}) \psi'_-(\delta\vec{p}) \right) \left( \bar{\psi}'_+(\delta\vec{k}) \psi'_-(\delta\vec{k} + \vec{q} + 2Q\vec{n}) \right) \\ & \quad \times \theta\left(\Lambda_f^2 - (\delta\vec{p} - \delta\vec{k} - 2Q\vec{n})^2\right). \end{aligned} \quad (45)$$

In contrast to the dominant terms, subdominant interactions require that at least one fermion must go far away from the Fermi surface regardless of any  $\vec{q}$ . The propagation of such a fermion serves the  $1/Q$  suppression in the quantum corrections.

#### 4.2 Formal Treatment: Bosonization

Now let us introduce the mean-field Ansatz for one patch. The auxiliary-field method may be applied as before. There are two slight modifications on the standard approach. One is that our boson field is introduced as a complex field since we need to eliminate quark bilinears,  $\bar{\psi}_+\psi_-$  and  $\bar{\psi}_-\psi_+$ , which have complex phase factors that are opposite to each other. Another is that boson fields are used to be replaced with only dominant four-Fermi interactions.

Inserting an identity to the original partition function, we introduce the bosonic terms,

$$\mathcal{S}_\Phi = -\frac{N_c}{2G} \int dx_0 \int_{p,q,k} \Phi^\dagger(\vec{q}; \vec{p}, x_0) \theta_{p,k} \Phi(\vec{q}; \vec{k}, x_0), \quad (46)$$

to the original action. For the moment, we will explicitly write the  $x_0$  coordinate. We replace the dominant four-Fermi interaction with a Yukawa-type vertex by shifting the boson fields,

$$\begin{aligned} \Phi^\dagger(\vec{q}; \vec{p}, x_0) &\longrightarrow \Phi^\dagger(\vec{q}; \vec{p}, x_0) + \frac{2G}{N_c} \bar{\psi}_+(\vec{p} + \vec{q}, x_0) \psi_-(\vec{p}, x_0), \\ \Phi(\vec{q}; \vec{k}, x_0) &\longrightarrow \Phi(\vec{q}; \vec{k}, x_0) + \frac{2G}{N_c} \bar{\psi}_-(\vec{k}, x_0) \psi_+(\vec{k} + \vec{q}, x_0), \end{aligned} \quad (47)$$

then the Yukawa vertex is

$$\begin{aligned} \mathcal{S}_{\Phi,\psi} = & - \int dx_0 \int_{p,q} \left[ \int_k \theta_{p,k} \Phi(\vec{q}; \vec{k}, x_0) \right] \bar{\psi}_+(\vec{p} + \vec{q}, x_0) \psi_-(\vec{p}, x_0) \\ & - \int dx_0 \int_{p,q} \left[ \int_k \theta_{p,k} \Phi^\dagger(\vec{q}; \vec{k}, x_0) \right] \bar{\psi}_-(\vec{p}, x_0) \psi_+(\vec{p} + \vec{q}, x_0), \end{aligned} \quad (48)$$

where terms inside of  $[\dots]$  in the first and second terms are the self-energy,  $\Sigma_m^\dagger(-\vec{q}; \vec{p})$  and  $\Sigma_m(\vec{q}; \vec{p})$ , respectively. And the equation of motion is

$$\begin{aligned} \langle \Phi(\vec{q}; \vec{k}) \rangle &= -\frac{2G}{N_c} \langle \bar{\psi}_-(\vec{k}, x_0) \psi_+(\vec{k} + \vec{q}, x_0) \rangle, \\ \langle \Phi^\dagger(\vec{q}; \vec{k}) \rangle &= -\frac{2G}{N_c} \langle \bar{\psi}_+(\vec{k} + \vec{q}, x_0) \psi_-(\vec{k}, x_0) \rangle. \end{aligned} \quad (49)$$

The RHS will appear to be  $x_0$  independent, so we will not have to write the  $x_0$  coordinate in  $\langle \Phi(\vec{q}; \vec{k}) \rangle$  and  $\langle \Phi^\dagger(\vec{q}; \vec{k}) \rangle$  anymore. Below we will not explicitly write  $x_0$  dependence of fermion fields for notational simplicity.

### 4.3 Mean Field for Chiral Spirals and the Quasi-Particle Spectrum

According to the arguments around Eq. (44), in the high-density limit the Ansatz for chiral spirals in the  $i$ -th patch is<sup>15</sup>

$$\Phi_0(\vec{q}; \vec{k}) = (2\pi)^2 \delta(\vec{q} - 2Q\vec{n}_i) \Delta(\vec{k}), \quad \Phi_0^\dagger(\vec{q}; \vec{k}) = (2\pi)^2 \delta(\vec{q} - 2Q\vec{n}_i) \Delta(\vec{k}), \quad (50)$$

where  $\Delta$  is a real field which characterizes the magnitude of the condensate. We will give what would happen if we chose different  $\vec{q}$  in Appendix A. The Fourier transformation with respect to the total momentum of the boson fields gives the expression,

$$\Phi_0(\vec{x}; \vec{k}) = \Delta(\vec{k}) e^{2iQx_\parallel}, \quad \Phi_0^\dagger(\vec{x}; \vec{k}) = \Delta(\vec{k}) e^{-2iQx_\parallel}, \quad (51)$$

from which we can see that the complex nature of the boson fields is taken into account in the phase factor.

For later convenience, let us define the mass gap function,

$$M(\vec{p}) \equiv \int_k \theta_{p,k} \Delta(\vec{k}), \quad (52)$$

which will be determined self-consistently after constructing the mean-field propagator. Using this shorthand notation and shifting momentum  $\vec{p} \rightarrow \vec{p} +$

<sup>15</sup> In our definition of  $\Phi^\dagger(\vec{q}; \vec{k})$  in Eq.(46),  $\Phi^\dagger(\vec{q}; \vec{k})$  actually carries momentum  $-\vec{q}$ .



$Q\vec{n}_i$ , the mass vertex becomes

$$\begin{aligned} \mathcal{S}_{\Phi,\psi} &\rightarrow \mathcal{S}_M = - \int dx_0 \int_p \left( M(\vec{p} - Q\vec{n}_i) \bar{\psi}_+(\vec{p} + Q\vec{n}_i) \psi_-(\vec{p} - Q\vec{n}_i) \right. \\ &\quad \left. + M(\vec{p} - Q\vec{n}_i) \bar{\psi}_-(\vec{p} - Q\vec{n}_i) \psi_+(\vec{p} + Q\vec{n}_i) \right) \\ &= - \int dx_0 \int_{\delta\vec{p}} \left( M'(\delta\vec{p}) \bar{\psi}'_+(\delta\vec{p}) \psi'_-(\delta\vec{p}) + M'(\delta\vec{p}) \bar{\psi}'_-(\delta\vec{p}) \psi'_+(\delta\vec{p}) \right). \end{aligned} \quad (53)$$

In the last line of the above equation, we have replaced the loop momentum  $\vec{p}$  with  $\delta\vec{p}$  and have defined  $M'(\delta\vec{p}) \equiv M(\delta\vec{p} - Q\vec{n}_i)$ .

Here it is very important to notice that although our inhomogeneous condensate breaks the translational invariance, momenta measured from the Fermi surface,  $\delta\vec{p}$ , is a conserved quantity. This is true as far as we include only dominant terms. The conservation of  $\delta\vec{p}$  is violated by corrections such as transverse kinetic terms or subdominant parts of four-Fermi interactions, but they are subleading effects suppressed by powers of  $1/Q$ .

At leading order, thanks to the conservation of  $\delta\vec{p}$ , the eigenvalue problem is diagonal in momentum space. Then we can formally derive the mean-field spectrum of quasi-particles using the mass function  $M'(\delta\vec{p})$ . The eigenvalue problem for the longitudinal plus mass terms is<sup>16</sup>

$$\Psi^\dagger \begin{pmatrix} \delta p_{\parallel} + Q & M'(\delta\vec{p}) \\ M'(\delta\vec{p}) & -\delta p_{\parallel} + Q \end{pmatrix} \Psi'(\delta\vec{p}) = E_{\text{MF}}(\delta\vec{p}) \left( \Psi^\dagger \Psi'(\delta\vec{p}) \right), \quad (54)$$

where a notation,  $\Psi'(\delta p_{\parallel}) = (\psi'_+(\delta\vec{p}), \psi'_-(\delta\vec{p}))^T$ , is introduced. The eigenvalue has upper and lower branches,

$$E_{\text{MF}}(\delta\vec{p}) = Q \pm \omega(\delta\vec{p}), \quad \left( \omega(\delta\vec{p}) = \sqrt{\delta p_{\parallel}^2 + M'(\delta\vec{p})^2} \right), \quad (55)$$

where the gap opens at  $|p_{\parallel}| = Q$ , and its influence survives up to distance  $\sim \Lambda_c$  from the Fermi surface. (For the case that the chiral spiral has a wave vector  $Q' \neq Q$ , see Appendix A.) Since the energy level for particles with a mass gap is pushed down as compared to free particles, the energy gain inside of one patch is  $\sim M \times (\text{phase space}) = M \times \Lambda_c Q \tan \Theta$ . Also, note that the phase space does not change before and after the formation of the mass gap, so that the Fermi volume conservation is automatically satisfied.

It is important to specify the relation between these upper and lower branches and the respective momentum regions. They can be summarized as

$$E_{\nearrow} = Q + \omega(\delta p_{\parallel}) \quad (p_{\parallel} > Q), \quad E_{\searrow} = Q - \omega(\delta p_{\parallel}) \quad (p_{\parallel} < Q), \quad (56)$$

<sup>16</sup> When we write  $2 \times 2$  matrix expressions, that means that each element is proportional to the  $2 \times 2$  identity matrix,  $\mathbf{1}_{2 \times 2}$ .

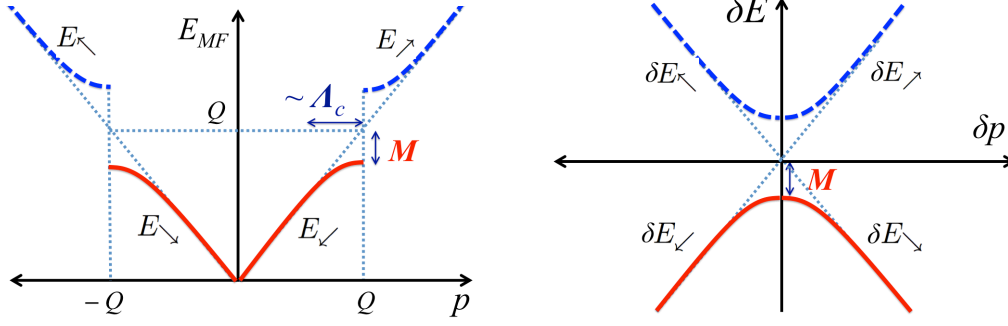


Fig. 11. The mean-field single-particle dispersion in the presence of the chiral spirals. The particle orbit is occupied up to  $|p_{\parallel}| \leq Q$ . The Fermi volume conservation is satisfied before and after the formation of chiral spirals. (Left) The energy  $E_{MF}$  in the  $\psi$ -representation. The gap opens at the edge of the Fermi surface. (Right) The energy  $\delta E = E_{MF} - Q$  in the  $\psi'$ -representation.

for states moving to the + direction, and

$$E_{\nwarrow} = Q + \omega(\delta p_{\parallel}) \quad (p_{\parallel} < -Q), \quad E_{\swarrow} = Q - \omega(\delta p_{\parallel}) \quad (p_{\parallel} > -Q), \quad (57)$$

for states moving to the - direction. See Fig. 11 for a graphical summary.

In Appendix A, we repeat calculations for  $\vec{q} \neq 2Q\vec{n}$ , and explain that at sufficiently high density, the choice  $\vec{q} = 2Q\vec{n}$  is the best way to minimize the single-particle contributions with the fixed particle number constraint.

#### 4.4 The Mean-Field Propagator in the Canonical Ensemble

Let us construct the mean-field propagator for the quasi-particle. We are working in the canonical ensemble with a fixed shape of the Fermi sea, i.e. one wedge, filled with quasi-particles up to  $|p_{\parallel}| \leq Q$ . This can be restated as the condition that all occupied states must take the lower energy branch of the mean-field spectra,  $E = Q - \omega$ . To take into account such information in the propagator, we have only to take a proper  $i\epsilon$  prescription as we usually do in the vacuum case.

The dominant fermion bilinear part of the action (longitudinal plus mass terms) is

$$\mathcal{S}_{\psi'}^{\parallel+M} = \int dp_0 \int_{\delta p} \bar{\Psi}'(p_0, \delta \vec{p}) \left( (p_0 - Q)\gamma^0 + \delta p_{\parallel}\gamma^{\parallel} - M'(\delta \vec{p}) \right) \Psi'(p_0, \delta \vec{p}). \quad (58)$$

Note that  $Q$  couples  $\gamma^0$ , not to  $\gamma^{\parallel}$ , as a consequence that we measure momenta of  $\psi_{\pm}$  in an opposite way. Defining  $\delta p_0 = p_0 - Q$ , our mean-field propagator

in the region of condensation is,

$$\mathcal{S}_{\text{MF}}(\delta p) = i \frac{\delta p_0 \gamma^0 + \delta p_{\parallel} \gamma^{\parallel} + M'(\delta \vec{p})}{(\delta p_0)^2 - (\delta p_{\parallel})^2 - M'^2(\delta \vec{p}) + i\epsilon} \cdot \theta_{\perp}(\delta \vec{p}), \quad (59)$$

and out of the condensation region, it is just a free quark propagator. Here  $i\epsilon$  is introduced as in the vacuum case in order to classify the propagations of particles in the upper and the lower energy branches. The last function  $\theta_{\perp}$  takes into account the phase space restriction of one wedge,

$$\begin{aligned} \theta_{\perp}(\delta \vec{p}) &\equiv \theta(|Q + \delta p_{\parallel}| \tan \Theta - |p_{\perp}|) \theta(|Q - \delta p_{\parallel}| \tan \Theta - |p_{\perp}|) \\ &\simeq \theta(Q \tan \Theta - |p_{\perp}|) \quad (\text{for } Q \gg |\delta p_{\parallel}|). \end{aligned} \quad (60)$$

This means that both quasi-particles and holes must be within one wedge to create chiral spirals. For the most part, we will assume the approximate expression in the second line, provided that  $Q$  is sufficiently large.

In the following, we will frequently use the component expression which is defined as

$$\mathcal{S}_{\text{MF}}(\delta p) = \begin{pmatrix} S_{++} & S_{+-} \\ S_{-+} & S_{--} \end{pmatrix} = \begin{pmatrix} \frac{1 + \Gamma_5}{2} \mathcal{S}_{\text{MF}} & \frac{1 - \Gamma_5}{2} & \frac{1 + \Gamma_5}{2} \mathcal{S}_{\text{MF}} & \frac{1 + \Gamma_5}{2} \\ \frac{1 - \Gamma_5}{2} \mathcal{S}_{\text{MF}} & \frac{1 - \Gamma_5}{2} & \frac{1 - \Gamma_5}{2} \mathcal{S}_{\text{MF}} & \frac{1 + \Gamma_5}{2} \end{pmatrix}. \quad (61)$$

Some useful component expression is given also in Appendix B.

#### 4.5 The Gap Equation and Its (1+1) Dimensional Character

Since we already have the formal expression of the propagator, we can now write the gap equation explicitly. The equation is (with the trace for the Dirac indices<sup>17</sup>),

$$\begin{aligned} M'(\delta \vec{p}) &= 2G \int \frac{d\delta k_0}{2\pi} \int_{\delta k} \theta_{\delta p, \delta k} \text{tr} \left[ \frac{iM'(\delta \vec{k})}{(\delta k_0)^2 - (\delta k_{\parallel})^2 - M'^2(\delta \vec{k}) + i\epsilon} \right] \theta_{\perp}(\delta \vec{k}) \\ &= 4G \int \frac{d\delta k_{\parallel} d\delta k_{\perp}}{(2\pi)^2} \frac{M'(\delta \vec{k})}{\sqrt{\delta k_{\parallel}^2 + M'^2(\delta \vec{k})}} \theta_{\delta p, \delta k} \theta_{\perp}(\delta \vec{k}). \end{aligned} \quad (62)$$

When we treat the self-consistent equation, we have to distinguish two situations depending on the fermion momenta. One case is that  $p_{\perp}$  resides suffi-

<sup>17</sup> Here we remind readers that we are using four component spinors, so the trace gives a factor 4.

ciently far from the patch boundary. The other case is that  $p_\perp$  is so close to the boundary that its mass gap is affected by other patches.

In this section, we focus only on the former case without the boundary effects and postpone the discussion on the latter case to the later sections, which actually goes beyond the one-patch problem.

For  $\vec{p}_\perp$  sufficiently far from the patch boundary, the restriction  $\theta_\perp(\vec{\delta k})$  is automatically satisfied by the other restriction  $\theta_{\delta p, \delta k}$ , so the former does not play any essential role. Then the gap equation has (1+1)-dimensional solutions. Indeed, we can find the mass gap function independent of  $p_\perp$ ,

$$M'_0(\delta \vec{p}) = M'_0(\delta p_\parallel). \quad (63)$$

When we look for such a solution, we can factorize the integral over  $k_\perp$ , which gives the (1+1)-dimensional gap equation,

$$\begin{aligned} M'_0(\delta p_\parallel) &= 4G \int \frac{d\delta k_\parallel}{2\pi} \frac{M'_0(\delta k_\parallel)}{\sqrt{\delta k_\parallel^2 + M_0'^2(\delta k_\parallel)}} \int \frac{d\delta k_\perp}{2\pi} \theta_{\delta p, \delta k} \\ &= \frac{4G}{\pi} \int_{\delta p_\parallel - \Lambda_f}^{\delta p_\parallel + \Lambda_f} \frac{d\delta k_\parallel}{2\pi} \frac{M'_0(\delta k_\parallel)}{\sqrt{\delta k_\parallel^2 + M_0'^2(\delta k_\parallel)}} \cdot \sqrt{\Lambda_f^2 - (\delta p_\parallel - \delta k_\parallel)^2}, \end{aligned} \quad (64)$$

where the  $p_\perp$  dependence disappears from the RHS as it should be.

Let us note that this factorization could not yield the  $p_\perp$ -independent solutions if we did not ignore corrections from the transverse kinetic terms  $\sim p_\perp^2/Q$  or  $\theta_\perp(\vec{\delta k})$ . If one of such terms become relevant, then the  $p_\perp$  dependence of the RHS does not disappear in the above manipulations. This means that the (1+1)-dimensional mass function can be obtained only if  $Q$  is sufficiently large and  $p_\perp$  is not too close to the one-patch boundary.

Now let us show that the non-trivial gap arises from the IR effects near the Fermi surface. We shall consider the case with  $\delta p_\parallel = 0$ . If we separate the integral region of the RHS into regions below and above a certain scale  $c\Lambda_f$  such that the momentum dependence in  $M'_0$  can be ignored below  $c\Lambda_f$ . Assuming that  $c\Lambda_f < \Lambda_f$ , we have

$$\begin{aligned} M'_0(0) &\simeq \frac{8G\Lambda_f}{\pi} \int_0^{c\Lambda_f} \frac{d\delta k_\parallel}{2\pi} \frac{M'_0(0)}{\sqrt{\delta k_\parallel^2 + M_0'^2(0)}} + (\text{finite positive terms}) \\ &= M'_0(0) \cdot \frac{4G\Lambda_f}{\pi^2} \ln \left( \frac{c\Lambda_f}{M'_0(0)} \right) + (\text{finite positive terms}), \end{aligned} \quad (65)$$

where the logarithmic term comes from the (1+1)-dimensional character of the equation, and expresses the IR effects.

In the same way as the Cooper instability in superconductivity, we can find the solution of the gap equation from the IR structure of the equation. Indeed, if we take  $M'_0(0)$  too small, the logarithmic part is divergingly large and the RHS exceeds the LHS much. Thus  $M'_0(0)$  must be taken substantially large until the IR contributions are tempered to be the same order of the LHS.

We point out that one oversimplification in the above expression is related to our approximation to ignore the transverse kinetic terms. If we recover those kinetic terms, the logarithmic part must be modified effectively as

$$\ln\left(\frac{c\Lambda_f}{M'_0(0)}\right) \rightarrow \ln\left(\frac{c\Lambda_f}{M'_0(0) + p_\perp^2/Q}\right), \quad (66)$$

which tempers the growth in the IR region. Thus, the gap solution might not be found unless the density is sufficiently large.

Finally, as a solution of the gap equation,  $M'_0$  is parametrically given as

$$M'_0 \sim \Lambda_f e^{-C/G\Lambda_f}, \quad (67)$$

where  $C$  is some number. Within our approximation, the size of the gap should be at least larger than that in vacuum because of larger phase space for low energy excitations which contribute to the formation of the gap.

## 5 Perturbation Theory with Chiral Spiral Mean Fields

In this section we develop systematic computation of the corrections from subdominant terms up to the leading order of the  $1/N_c$  expansion.

Using the stationary phase approximation at large  $N_c$ , the fermionic partition function under chiral spiral backgrounds for fixed  $\Theta$  is

$$\begin{aligned} Z_\psi[\langle\Phi\rangle, \Theta] &= \int \mathcal{D}\psi' \mathcal{D}\bar{\psi}' e^{i(\mathcal{S}_{\text{MF}} + \Delta\mathcal{S})} \\ &= Z_{\text{MF}} \left\langle 1 + i\Delta\mathcal{S} + \frac{i^2}{2!}(\Delta\mathcal{S})^2 + \dots \right\rangle_{\text{MF}}, \end{aligned} \quad (68)$$

where  $\langle\cdots\rangle_{\text{MF}}$  is the expectation value when we use the mean-field weight,  $e^{i\mathcal{S}_{\text{MF}}}$ , in the path integral. The action is made of

$$\begin{aligned} \mathcal{S}_{\text{MF}} &= \sum_i \left( \mathcal{S}_i^{\parallel+M} + \mathcal{S}_i^\Phi \right), \\ \Delta\mathcal{S} &= \sum_i \left( \mathcal{S}_i^\perp + \mathcal{S}_i^{\text{sub.int}} \right) + \sum_{i \neq j} \mathcal{S}_{i,j} + \sum_{i,j \neq k} \mathcal{S}_{i,j,k} + \sum_{i \neq j, k \neq l} \mathcal{S}_{i,j,k,l}, \end{aligned} \quad (69)$$

where  $\mathcal{S}_{\text{MF}}$  is the mean-field action which is the (uncorrelated) sum of one-patch actions. The  $\mathcal{S}_i^\perp$  and  $\mathcal{S}_i^{\text{sub.int}}$  are subdominant terms inside of the  $i$ -th patch, which were not treated in the last section. Finally  $\mathcal{S}_{i,j}, \dots$  describe the interactions among different patches.

The energy density functional is given by  $\mathcal{E}[\langle\Phi\rangle, \Theta] = -i \ln Z/\mathcal{V}_3 = \mathcal{E}_{\text{MF}} + \Delta\mathcal{E}$  (with  $\mathcal{V}_3$  being the (2+1)-dimensional space-time volume), where

$$\mathcal{E}_{\text{MF}} = \frac{-i}{\mathcal{V}_3} \ln Z_{\text{MF}}, \quad \Delta\mathcal{E} = \frac{-i}{\mathcal{V}_3} \cdot \left\langle i\Delta\mathcal{S} + \frac{i^2}{2!}(\Delta\mathcal{S})^2 + \dots \right\rangle_{\text{MF}}^{\text{conn.}}. \quad (70)$$

We wish to measure the energy benefit from the chiral spiral formations. To do so, we need to subtract the energy of the trivial configuration, and so we should compute,

$$\delta\mathcal{E}[\langle\Phi\rangle, \Theta] = \mathcal{E}[\langle\Phi\rangle, \Theta] - \mathcal{E}[0, 0]. \quad (71)$$

When we apply the perturbative expansion soon later, it is convenient to reorganize the above expression into

$$\delta\mathcal{E}[\langle\Phi\rangle, \Theta] = \left( \mathcal{E}[\langle\Phi\rangle, \Theta] - \mathcal{E}[0, \Theta] \right) + \left( \mathcal{E}[0, \Theta] - \mathcal{E}[0, 0] \right). \quad (72)$$

The first term expresses genuine condensation effects, while the second term comes from the deformation energy, which was already computed at the introduction and turned out to be  $\sim p_{\text{F}}^3 \Theta^4$ . Our task below is the computation of the quantity inside of the first parentheses.

In the following, we will use the  $\psi'$ -representation. The advantage of doing this is that the momentum  $\delta p$  in the propagator is conserved, and we can express the propagator as a function of relative distance in space-time,  $x - y$ . Noting this fact, many of diagrams can be easily cast away. Let us recall that the subdominant terms have oscillating factors multiplied to the fermion fields. Non-zero contributions remain only if the combination of vertices has the oscillating factors in a form of  $e^{\pm iQ(x-y)_\parallel}$ ,  $e^{\pm 2iQ(x-y)_\parallel}$ ,  $\dots$  because propagators are functions of  $x - y$ . In other words, this is simply a consequence of the momentum conservation in our shifted variables.

For example, let us see the first-order expansion, that gives a tadpole contribution, such as

$$\int d^3x \left( \left\langle \bar{\psi}'_+ i\partial_\perp \psi'_- \right\rangle_{\text{MF}} e^{-2iQx_\parallel} + \left\langle \bar{\psi}'_- i\partial_\perp \psi'_+ \right\rangle_{\text{MF}} e^{2iQx_\parallel} \right). \quad (73)$$

This is, however, a space-independent quantity times an oscillation factor, and so its spatial integral vanishes for  $Q \neq 0$ . This is an example of the momentum conservation. Non-zero correction terms start to arise from the second order of the perturbative expansion.

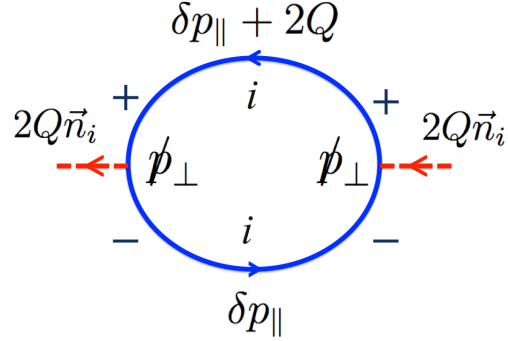


Fig. 12. A diagram for the transverse kinetic terms in the  $i$ -th patch. Here we used the  $\psi'$ -representation in which  $\psi'$  fields effectively feel incoming and outgoing momenta,  $2Q\vec{n}_i$ . This makes at least one fermion go far away from the Fermi surface.

In the following, we will first compute the corrections from one patch which include transverse kinetic terms and subdominant four-Fermi interactions in one patch. Second, we will compute interaction terms including patch-patch interactions.

## 6 Corrections from One Patch

We consider the perturbative corrections inside of the  $i$ -th patch. For the moment we will omit the subscript  $i$ . The sources of second-order corrections are enumerated as follows: (1) (transverse terms)<sup>2</sup>, (2) (four-Fermi interaction terms)<sup>2</sup>, (3) (transverse terms)  $\times$  (four-Fermi interaction terms). The last one, (3), cannot cancel oscillating factors out, and only (1) and (2) contribute to the free energy.

### 6.1 Product of Transverse Kinetic Terms

The non-zero contributions from the product of transverse terms arise from  $(+-)(-+)$  or  $(-+)(+-)$  combinations, i.e.

$$\begin{aligned}
\Delta\mathcal{E}_{\text{trans}} &= \frac{i}{\mathcal{V}_3} \int d^3x d^3y \left\langle [\bar{\psi}'_+ i\cancel{\partial}_{\perp} \psi'_-(x)] [\bar{\psi}'_- i\cancel{\partial}_{\perp} \psi'_+(y)] \right\rangle_{\text{MF}} e^{-2iQ(x-y)_{\parallel}} \\
&= N_c \int \frac{d^2\delta p}{(2\pi)^2} p_{\perp}^2 \int \frac{d\delta p_0}{2\pi} \\
&\quad \times (-i) \text{tr} \left[ S_{--}(\delta p_0, \delta p_{\parallel}, p_{\perp}) S_{++}(\delta p_0, \delta p_{\parallel} + 2Q, p_{\perp}) \right]. \tag{74}
\end{aligned}$$

After the  $p_0$  integration, we have

$$\Delta\mathcal{E}_{\text{trans}} = N_c \int \frac{d\delta p_{\parallel}}{2\pi} \int_{\theta_1(Q)} \frac{dp_{\perp}}{2\pi} p_{\perp}^2 \cdot \frac{F(\delta p_{\parallel}, 2Q)}{\omega(\delta p_{\parallel}) + \omega(\delta p_{\parallel} + 2Q)}, \quad (75)$$

where the integral of the transverse momentum is restricted within one patch,

$$\int_{\theta_1(Q)} \frac{dp_{\perp}}{2\pi} \equiv \int \frac{dp_{\perp}}{2\pi} \theta_{\perp}(\delta p_{\parallel}, p_{\perp}) \theta_{\perp}(\delta p_{\parallel} + 2Q, p_{\perp}), \quad (76)$$

and we defined the function  $F(\delta p_{\parallel}, 2Q)$  as

$$F(\delta p_{\parallel}, 2Q) = 1 + \frac{\delta p_{\parallel}}{\omega(\delta p_{\parallel})} \frac{\delta p_{\parallel} + 2Q}{\omega(\delta p_{\parallel} + 2Q)} \quad (0 \leq F \leq 2). \quad (77)$$

Now let us analyze Eq. (75). The key point is that at least one of the momenta,  $\delta p_{\parallel}$  or  $\delta p_{\parallel} + 2Q$ , must be much larger than  $\Lambda_c$ . If both of the momenta are much bigger than  $\Lambda_c$ , then the mass gap does not exist, so that the result is just reduced to the one in the free theory. It is thus a non-trivial case when one of the momenta is close to the Fermi surface. Let us consider such a situation in the following.

Supposing that  $|\delta p_{\parallel}| < \Lambda_c$ , the other momentum  $\delta p_{\parallel} + 2Q$  satisfies  $2Q - \Lambda_c < \delta p_{\parallel} + 2Q < 2Q + \Lambda_c$ . Therefore we can use the free fermion dispersion for  $\omega(\delta p_{\parallel} + 2Q) = \delta p_{\parallel} + 2Q$ , and can apply an approximate upper bound,  $Q \tan \Theta$ , for the  $p_{\perp}$ -integral.

In order to make physical interpretations, we should notice that generically the perturbative expansion contains the trivial contribution that is independent of the condensate, and this must be subtracted. Here we subtract such trivial contributions with the same phase space as the non-trivial one. Outside of the condensation domain, two contributions cancel out. After subtracting terms at  $M' = 0$ , the non-trivial contribution of Eq. (75) is given by

$$\begin{aligned} \Delta\mathcal{E}_{\text{trans}} &\simeq \frac{N_c}{\pi^2} \int_0^{\Lambda_c} d\delta p_{\parallel} \int_0^{Q \tan \Theta} dp_{\perp} \frac{p_{\perp}^2}{2Q} \left[ \left( 1 + \frac{\delta p_{\parallel}}{\sqrt{\delta p_{\parallel}^2 + M'^2(\delta p_{\parallel})}} \right) - 2 \right] \\ &\sim -N_c \cdot M' Q^2 \tan^3 \Theta \quad (M' \sim \Lambda_f), \end{aligned} \quad (78)$$

where  $-2$  in the first line represents the subtraction of the trivial contribution. Note that the energy correction before performing the integration is  $\sim p_{\perp}^2/Q$ , and so at the level of the computation of the fermion dispersion relation, this terms were negligible effects.

The sign of Eq. (78) is negative, which means that this term corresponds to an energy gain. This term can be regarded as a controllable correction only if



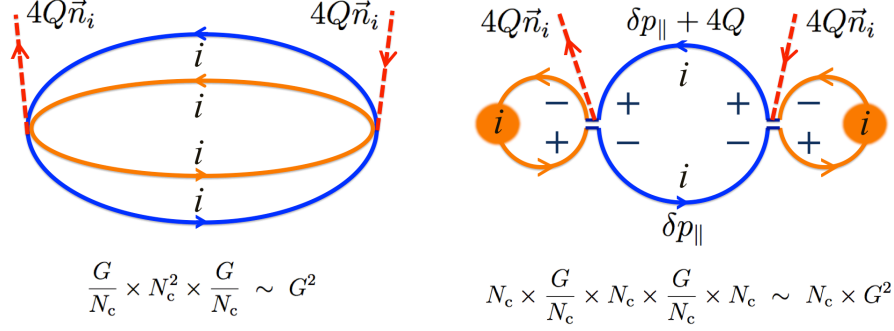


Fig. 13. Contributions from the subdominant vertices. The  $\psi'$ -representation is used and all fields belong to the  $i$ -th patch. (Left) The  $O(N_c^0)$  contribution which is ignored in this work. (Right) The  $O(N_c)$  contributions. The diagram can be interpreted as the condensate-condensate interaction mediated by particle-hole excitations. One of fermions in the internal loop must go far from the Fermi surface.

it is sufficiently smaller than the energy gain from the one-patch mean field,  $N_c \cdot \Lambda_f^2 Q \tan \Theta$ . This requires the condition,  $\Theta \ll (\Lambda_f/Q)^{1/2}$ , as already stated at the introduction.

Finally let us mention on how the perturbative analysis of the correction from the transverse kinetic energy can be organized in a systematic way. If we go to higher order of the transverse kinetic terms, we have terms of higher powers of  $p_\perp^2/Q$  in the integrand. Computing the  $p_\perp$ -integration with the integral region  $\sim Q \tan \Theta$  results in terms of higher powers of  $\Theta \ll 1$ , which appears as an expansion parameter in the systematic computations.

## 6.2 Product of Four-Fermi Interaction Terms

We will compute the second-order perturbation of subdominant four-Fermi interaction terms, which reads

$$\frac{i}{\mathcal{V}_3} \cdot \frac{G^2}{N_c^2} \int d^3x d^3y \langle (\bar{\psi}'_+ \psi'_-(x))^2 (\bar{\psi}'_- \psi'_+(y))^2 \rangle_{\text{MF}} e^{-4iQ(x-y)_\parallel}. \quad (79)$$

Equation (79) yields several distinct terms depending on how fermion lines are contracted. Here we introduce the hierarchy for different contractions by applying the  $1/N_c$  expansion. At large  $N_c$ , the dominant contributions come from condensate-condensate interactions mediated by virtual quark-hole exchange. This situation is schematically described as

$$\sim G^2 \frac{\langle \bar{\psi}'_+ \psi'_- \rangle_{\text{MF}}}{N_c} \left( (-i) N_c \int d^3z \text{tr} [S_{++}(z) S_{--}(-z)] e^{-4iQz_\parallel} \right) \frac{\langle \bar{\psi}'_- \psi'_+ \rangle_{\text{MF}}}{N_c} \quad (80)$$

with  $z = x - y$  (see the right panel in Fig. 13). Here the form factor is not explicitly written yet. This contribution is  $O(N_c)$  and positive, according to the previous calculations which treated the integral in the bracket. One fermion pair at  $x$  and  $y$  is contracted at one space-time point and becomes condensates. The remaining part is for the particle-hole propagation between  $x$  and  $y$ . Loosely speaking, this part can be interpreted as the propagation of meson-like objects with total momentum  $4Q$  (though ladder-type resummation is necessary to construct the meson propagation in fact).

Let us note that the size of the condensate of  $O(N_c)$  compensates for the suppression factor of  $O(1/N_c)$  in the intrinsic interaction vertex. Other contractions without the condensate cannot be accompanied by a fermion loop of  $O(N_c)$  and are suppressed by  $1/N_c$ .

We should not take Eq. (80) literally, however, since the loop integral is UV divergent, which is regulated with the form factor. It should be mentioned that such apparent UV divergence couples to the condensate, so the subtraction of the trivial configuration without the condensate cannot regulate the UV behavior.

Including the form factor explicitly and carrying out the integral in Eq. (79), we have

$$\begin{aligned} & \sim N_c G^2 \int_{\delta p, \delta k, \delta l} \theta(\Lambda_f^2 - (\delta \vec{p} - \delta \vec{k} + 2Q\vec{n})^2) \theta(\Lambda_f^2 - (\delta \vec{p} - \delta \vec{l} + 2Q\vec{n})^2) \\ & \times \left( \int d\delta k_0 \frac{\langle \bar{\psi}'_+ \psi'_-(\delta k) \rangle}{N_c} \right) \frac{F(\delta p_{\parallel}, 4Q)}{\omega(\delta p_{\parallel}) + \omega(\delta p_{\parallel} + 4Q)} \left( \int d\delta l_0 \frac{\langle \bar{\psi}'_- \psi'_+(\delta l) \rangle}{N_c} \right), \end{aligned} \quad (81)$$

or equivalently,

$$\sim N_c \int_{\delta p} M'(\delta \vec{p} + 2Q\vec{n}) \frac{F(\delta p_{\parallel}, 4Q)}{\omega(\delta p_{\parallel}) + \omega(\delta p_{\parallel} + 4Q)} M'(\delta \vec{p} + 2Q\vec{n}). \quad (82)$$

Here the phase-space restriction for the transverse momentum is not explicitly written. The condensate takes a finite value only if  $|\delta k_{\parallel}|, |\delta l_{\parallel}| < \Lambda_c$ . Once they are restricted within such a domain,  $\delta \vec{p}$  is also restricted around  $-2Q\vec{n}$ , and so the integral over the phase space has a UV cutoff. The integrand itself is suppressed by  $1/Q$ . Finally the energy cost from this contribution can be estimated as

$$(\text{one-patch energy cost}) \sim N_c \frac{\Lambda_f^2}{Q} \cdot \Lambda_f Q \tan \Theta \sim N_c \Lambda_f^3 \tan \Theta. \quad (83)$$

Here, a phase-space factor  $\sim \Lambda_f Q \tan \Theta$  arises because one spatial momentum is not restricted by the  $\theta$  function constraint in Eq. (81). As expected, this contribution is much smaller than the one-patch mean-field contribution  $\sim N_c \cdot \Lambda_f^2 Q \tan \Theta$ , so can be safely ignored at large density.

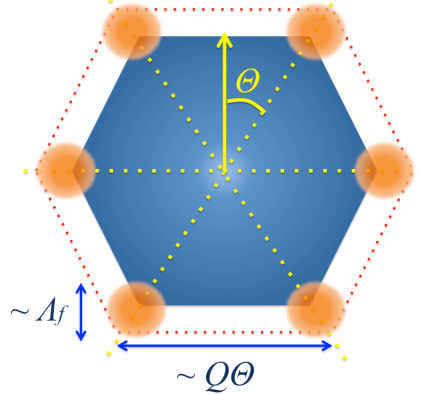


Fig. 14. The domain where the chiral spiral mean field in one patch couples to particles (holes) in its nearest neighbor patches. The size of such a domain is  $\sim \Lambda_f^2$  due to form factor effects.

## 7 Contributions from Patch Boundaries: Inter-Patch Effects

So far, we have ignored the interactions among fermions belonging to different patches. Due to the form-factor effects, such interactions occur only near the boundaries of patches. We will discuss the impact of such effects.

The outline for our computational procedure is the following. The condensation effects generate the following three types of the energy contributions,

$$\mathcal{E}_{\text{cond.}} \sim N_p \left( \mathcal{E}_{\text{inside}}^{\text{1-patch}}(M_0, \Theta) + \mathcal{E}_{\text{B}}^{\text{1-patch}}(M_{\text{B}}, \Theta) + \mathcal{E}_{\text{int}}^{\text{patches}}(M_{\text{B}}, \Theta) \right), \quad (84)$$

where  $\mathcal{E}_{\text{inside}}^{\text{1-patch}}$  and  $\mathcal{E}_{\text{B}}^{\text{1-patch}}$  are one-patch condensation energy in the region far from and close to the boundaries, and  $\mathcal{E}_{\text{int}}^{\text{patches}}$  represents the patch-patch interaction at the boundaries. The subscript B means the boundary, and  $M_0$  and  $M_{\text{B}}$  can be considerably different. The energy density schematically behaves as

$$\begin{aligned} \mathcal{E}_{\text{cond.}}/N_c &\sim \frac{1}{\Theta} \left( -M_0 \Lambda_f (Q \tan \Theta - \Lambda_f) - M_{\text{B}} \Lambda_f^2 + \mathcal{E}_{\text{int}}^{\text{patches}}(M_{\text{B}}, \Theta) \right) \\ &\sim -M_0 \Lambda_f Q + \frac{1}{\Theta} \left( \Lambda_f^2 (M_0 - M_{\text{B}}) + \mathcal{E}_{\text{int}}^{\text{patches}}(M_{\text{B}}, \Theta) \right). \end{aligned} \quad (85)$$

We will show that  $\mathcal{E}_{\text{int}}^{\text{patches}}$  is positive (at least at the level of the second-order perturbation theory). Its strength is determined by the size of  $M_{\text{B}}$ , and vanishes when  $M_{\text{B}} \rightarrow 0$ .

Equation (85) can be understood in twofold ways. If we regard the incoherent sum of the one-patch actions as our unperturbed action,  $M_{\text{B}}$  at the unperturbed level is  $\sim M_0$ , and  $\mathcal{E}_{\text{int}}^{\text{patches}}$  provides relatively large, positive contri-

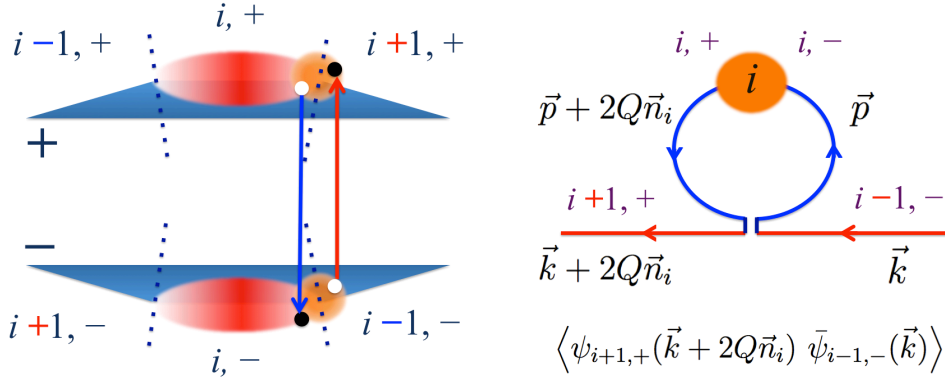


Fig. 15. (Left) An influence of the  $i$ -th chiral spiral mean-field at the patch boundaries. Only the Fermi surface close to  $i$ -th patch is shown. The  $i$ -th chiral spiral can scatter a particle (hole) state in the  $(i+1)$ -th patch into a hole (particle) state in the  $(i-1)$ -th patch. Such processes are possible only for a particle and a hole close to the  $i$ -th patch boundary. (Right) A diagrammatic expression of the particle-condensate scattering. The vector  $\vec{p}$  and  $\vec{k}$  must be close each other.

butions. This means that the inter-patch interactions between different chiral spirals reduce the energy gain from creating the condensates at the patch boundaries. Instead, if we assume  $M_B \ll M_0$ , then the one-patch contribution is  $M_0 - M_B \sim M_0 \sim \Lambda_f$ , while  $\mathcal{E}_{\text{int}}^{\text{patches}}$  is negligible. In both limiting cases, the sign of  $1/\Theta$  terms is positive and of  $O(\Lambda_f^3)$ .

The precise estimate of the  $1/\Theta$  term would be given by self-consistently solving the gap equation of  $M_B$  with  $\mathcal{E}_{\text{int}}^{\text{patches}}$ . This is beyond our scope in this paper. Instead, we will give several indicative discussions to understand inter-patch interactions at the patch boundaries, in both perturbative and non-perturbative manners.

### 7.1 Preliminaries

As we have already seen, at large  $N_c$ , the dominant correction terms come from condensate-condensate interactions mediated by virtual quark-hole excitations. Therefore we will take into account only such terms. Then we need consider only vertices in which two indices of the patches are identical, such as terms in  $\mathcal{L}_{i,j}^{\text{int}}$  or  $\mathcal{L}_{i,jk}^{\text{int}}$ .

Actually, because of the form factor, only a particle and a hole in  $(i \pm 1)$ -th patches can directly couple to the  $i$ -th chiral-spiral mean field. Therefore we

have only to consider the following types of the vertices (see also Fig. 15),

$$\int_{p,k} \langle \bar{\psi}_{i+}(\vec{p} + 2Q\vec{n}_i) \psi_{i-}(\vec{p}) \rangle \bar{\psi}_{i-1,-}(\vec{k}) \psi_{i+1,+}(\vec{k} + 2Q\vec{n}_i) \theta_{p,k}, \quad (86)$$

where we have replaced a fermion bilinear in the  $i$ -th patch with the chiral spiral mean field. Using the shifted momentum variables,  $\delta\vec{p} = \vec{p} + Q\vec{n}_i$  and  $\delta\vec{k} = \vec{k} + Q\vec{n}_{i-1}$ , and the  $\psi'$ -representation, Eq. (86) can be rewritten as

$$\int_{\delta p, \delta k} \langle \bar{\psi}'_{i+}(\delta\vec{p}) \psi'_{i-}(\delta\vec{p}) \rangle \bar{\psi}'_{i-1,-}(\delta\vec{k}) \psi'_{i+1,+}(\delta\vec{k} + Q(2\vec{n}_i - \vec{n}_{i-1} - \vec{n}_{i+1})) \\ \times \theta(\Lambda_f^2 - (\delta\vec{p} - \delta\vec{k} - Q\vec{n}_i + Q\vec{n}_{i-1})^2). \quad (87)$$

In perturbative computations, it is necessary to decompose momenta of the fermion field into the longitudinal and transverse components. Here let us briefly summarize necessary ingredients for the computations. Note that

$$\vec{n}_{i\pm 1} = \cos 2\Theta \vec{n}_i \mp \sin 2\Theta \vec{n}_{i\perp}, \quad \vec{n}_{i\pm 1,\perp} = \pm \sin 2\Theta \vec{n}_i + \cos 2\Theta \vec{n}_{i\perp}. \quad (88)$$

If we write  $\delta\vec{k} = \delta k_{\parallel} \vec{n}_{i-1} + k_{\perp} \vec{n}_{i-1,\perp}$ , then the momentum in  $\psi'_{i+1,+}$  can be decomposed into the  $\vec{n}_{i+1}$  and the  $\vec{n}_{i+1,\perp}$  directions,

$$\delta\vec{k} + Q(2\vec{n}_i - \vec{n}_{i-1} - \vec{n}_{i+1}) \\ = \left[ \delta k_{\parallel} \cos 4\Theta + k_{\perp} \sin 4\Theta + Q(2 \cos 2\Theta - \cos 4\Theta - 1) \right] \vec{n}_{i+1} \\ + \left[ -\delta k_{\parallel} \sin 4\Theta + k_{\perp} \cos 4\Theta + Q(-2 \sin 2\Theta + \sin 4\Theta) \right] \vec{n}_{i+1,\perp} \\ \simeq (\delta k_{\parallel} + 4k_{\perp} \Theta) \vec{n}_{i+1} + k_{\perp} \vec{n}_{i+1,\perp} + O(\delta k_{\parallel} \Theta, Q\Theta^2), \quad (89)$$

where we did not explicitly write quantities which are much smaller than  $\Lambda_f$ . Similarly, let us simplify the expression of the argument in the form factor. A decomposition of the momentum,

$$\delta\vec{p} - \delta\vec{k} - Q\vec{n}_i + Q\vec{n}_{i-1} \\ = \left[ \delta p_{\parallel} - \delta k_{\parallel} \cos 2\Theta - k_{\perp} \sin 2\Theta + Q(\cos 2\Theta - 1) \right] \vec{n}_i \\ + \left[ p_{\perp} - k_{\perp} \cos 2\Theta + \delta k_{\parallel} \sin 2\Theta - Q \sin 2\Theta \right] \vec{n}_{i+1,\perp} \\ \simeq (\delta p_{\parallel} - \delta k_{\parallel}) \vec{n}_i + (p_{\perp} - k_{\perp} - 2Q\Theta) \vec{n}_{i\perp} + O(\delta k_{\parallel} \Theta, Q\Theta^2), \quad (90)$$

leads to

$$\theta(\Lambda_f^2 - (\delta p_{\parallel} - \delta k_{\parallel})^2 - (p_{\perp} - k_{\perp} - 2Q\Theta)^2). \quad (91)$$

The  $\theta$  function is non-zero only around the patch boundary, that is,  $p_{\perp} \sim Q\Theta$  and  $k_{\perp} \sim -Q\Theta$ .

Finally let us note that the projection operators in one patch are different

from those in other patches. Indeed,

$$\begin{aligned} \frac{1 + \Gamma_{i+1,5}}{2} \cdot \frac{1 - \Gamma_{i-1,5}}{2} &= \frac{1 + \gamma_0 \gamma_{i+1,\parallel}}{2} \cdot \frac{1 - \gamma_0 (\gamma_{i+1,\parallel} \cos 2\Theta - \gamma_{i+1,\perp} \sin 2\Theta)}{2} \\ &= \left( (1 - \cos 2\Theta) + \sin 2\Theta \gamma_0 \gamma_{i+1,\perp} \right) \frac{1 + \Gamma_{i+1,5}}{4}, \end{aligned} \quad (92)$$

and

$$\frac{1 \pm \Gamma_{i+1,5}}{2} \cdot \frac{1 \pm \Gamma_{i-1,5}}{2} = \frac{1 \pm \Gamma_{i+1,5}}{4} \left( (1 + \cos 2\Theta) \mp \sin 2\Theta \gamma_0 \gamma_{i+1,\perp} \right). \quad (93)$$

In what follows, these slight modifications provide only negligible contributions of  $O(\Theta)$ , so we need not care them seriously in the computations.

## 7.2 Perturbative Consideration

The purpose of this subsection is to get the typical size of patch-patch interactions, and more importantly, to investigate whether interactions are attractive or repulsive. The latter can be done even without detailed estimates of the gap near the patch boundaries.

The perturbative computations proceed in almost exactly the same way as before. After taking the residue, we have an expression analogous to Eq. (82),

$$N_c \int_{\delta k} M_B'^2(\delta k_{\parallel}, k_{\perp} + 2Q\Theta) \frac{F_B(\delta k_{\parallel}, 4k_{\perp}\Theta)}{\omega_B(\delta k_{\parallel}) + \omega_B(\delta k_{\parallel} + 4k_{\perp}\Theta)} \geq 0, \quad (94)$$

where  $0 \leq F_B \leq 2$  by definition of Eq. (82), and  $k_{\perp} \sim -Q\Theta$ . The product of  $M_B'$  comes from the condensates (i.e. fermion loops) in the  $i$ -th patch, and the remaining piece comes from virtual particle-hole excitations. We emphasize that for the momentum conservation to be satisfied, both condensates must come from the same patch. The subscript B is attached to remind that the sizes of the gap and mass function near the boundaries may be considerably different from those far from the boundaries.

The sign is positive, so this is an energy cost. Although this is nothing beyond a generic fact inherent to the second-order perturbation, it indicates that boundary effects tend to temper the magnitude of the condensates near the boundaries.

It is very important to notice that the energy cost may be comparable to the energy gain from forming a condensate within the same phase space  $\sim \Lambda_f^2$ . In contrast to the case of subdominant terms, we do not have  $1/Q$  suppression

because all fermions can move around the Fermi surface during the virtual processes.

Let us investigate the order of the magnitude. If we assumed  $M'_B \gg Q\Theta^2$ , we can make an approximation that

$$(\text{Integrand in Eq. (94)}) \sim \frac{M_B'^2}{\sqrt{\delta k_{\parallel}^2 + M_B'^2}} \left( 1 - \frac{\delta k_{\parallel} k_{\perp} \Theta}{\sqrt{\delta k_{\parallel}^2 + M_B'^2}} + \dots \right), \quad (95)$$

thus the integral of the above integrand in the IR region gives an approximate expression as

$$\Lambda_f M_B'^2 \left[ \ln \left( \frac{\Lambda_f}{M_B'} \right) + \frac{2Q\Theta^2}{\sqrt{\Lambda_f^2 + M_B'^2}} \dots \right] \sim M_B'^2 \left( \frac{1}{G} + O(Q\Theta^2) \right) \sim \Lambda_f^3, \quad (96)$$

where we have used  $G \sim \Lambda_f^{-1}$  and the parametric behavior of the mass gap,  $M_B' \sim \Lambda_f e^{-C/G\Lambda_f}$ . This expression indeed confirms that the energy cost is of the same order as the energy gain from condensation effects within the same phase space.

Unfortunately, any obvious expansion parameter did not appear for this perturbative expansion, so we have no good reason to cast away higher-order diagrams. For a more reasonable estimate, the non-perturbative computations are necessary to simultaneously treat patch-patch interactions and the mean-field problem near the patch boundaries.

### 7.3 Some Non-perturbative Considerations: A (1+1)-Dimensional Example of Two Chiral Spirals

To get some insights for the inter-patch interactions between several chiral spirals, let us consider the simplest (1+1)-dimensional example. We assume the mean field which has two chiral spirals with wavevectors  $Q_0$  and  $Q_1$ . We will see how these two chiral spirals affect each other.

The mean-field eigenvalue equation is

$$E_{\text{MF}} \Psi(x_{\parallel}) = \begin{pmatrix} i\partial_{\parallel} & M_0 e^{2iQ_0 x_{\parallel}} + M_1 e^{2iQ_1 x_{\parallel}} \\ M_0 e^{-2iQ_0 x_{\parallel}} + M_1 e^{-2iQ_1 x_{\parallel}} & -i\partial_{\parallel} \end{pmatrix} \Psi(x_{\parallel}),$$

where  $\Psi(x_{\parallel}) = (\psi_+(x_{\parallel}), \psi_-(x_{\parallel}))^T$  is defined as before.

We rewrite this expression in the  $\psi'$ -representation in order to eliminate the oscillating factors. When we have two chiral spirals, those oscillating factors cannot be eliminated simultaneously. If  $M_0 > M_1$ , it is better to eliminate

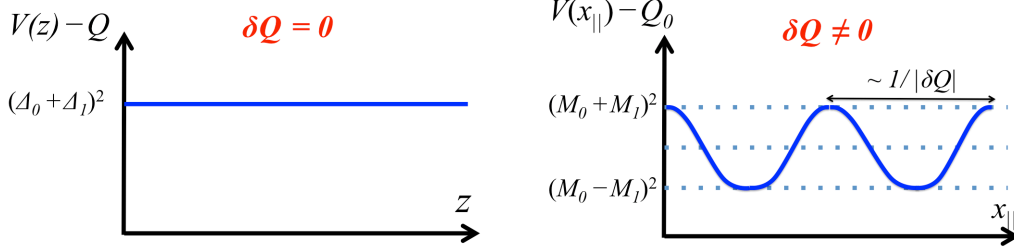


Fig. 16. The potential  $V(x_{\parallel}) - Q_0$ . (Left)  $\delta Q = 0$  case. The potential is constant. (Right)  $\delta Q \neq 0$  case. The potential is oscillating, so particles can stay around the valley of the potential. For very small  $\delta Q$ , its kinetic energy cost is small.

$e^{\pm 2iQ_0 x_{\parallel}}$ , as will be clear in the following. Using  $\psi_{\pm} = \psi'_{\pm} e^{\pm iQ_0 x_{\parallel}}$  and multiplying the Hamiltonian squared, we have the following Schrödinger equation,

$$(E_{\text{MF}} - Q_0)^2 \Psi'(x_{\parallel}) = \begin{pmatrix} \mathcal{H}'_{\text{diag.}} & 2\delta Q M_1 e^{2i\delta Q x_{\parallel}} \\ 2\delta Q M_1 e^{-2i\delta Q x_{\parallel}} & \mathcal{H}'_{\text{diag.}} \end{pmatrix} \Psi'(x_{\parallel}), \quad (97)$$

where  $\delta Q = Q_1 - Q_0$ , and

$$\mathcal{H}'_{\text{diag.}} = -\partial_{\parallel}^2 + (M_0 - M_1)^2 + 4M_0 M_1 \cos^2 \delta Q x_{\parallel}. \quad (98)$$

The off-diagonal Hamiltonian has the amplitude proportional to  $\delta Q M_1$ . Therefore, if  $|\delta Q|$  or  $M_1$  is small enough, one can ignore the off-diagonal part. Here one can understand that our choice to eliminate  $Q_0$  rather than  $Q_1$  is suited for this approximation since  $M_0 > M_1$ .

The diagonal part has a positive oscillating potential whose period is  $1/|\delta Q|$ ; see Fig. 16. A singularity lies at  $\delta Q = 0$  which leads to a constant potential, and the energy spectra are discontinuous from those at  $\delta Q \neq 0$ . If  $|\delta Q|$  is small enough but not zero, then we can find the eigenfunction whose kinetic energy is very small. That is,

$$E \sim Q_0 \pm |M_0 - M_1|, \quad (99)$$

for  $0 < |\delta Q| \ll M_0$ . When  $M_0$  is comparable to  $M_1$ , they nearly cancel each other, making the effective gap small. This analysis indicates that two chiral spirals with different but similar wave vectors tend to reduce the energy gain in single particle contributions.

If two chiral spirals have substantially different wavevectors, say,  $|\delta Q| \sim M$ , then the valley of the potential becomes narrow, and the kinetic energy is  $\sim M$ . In such a case inter-patch interactions do not strongly reduce the energy gain. This remark will be increasingly important when we consider the lower density region where higher harmonics of chiral spirals start to contribute because of the subdominant terms. We will discuss this in the next section.



## 8 Discussion

So far we have used the four-Fermi interaction which is strong enough to induce the chiral symmetry breaking near the Fermi surface. At the same time, we have relied on the high-density approximation to make our discussions simple enough to explore analytic insights. In reality with  $N_c = 3$ , however, gluons will be screened at high density, reducing the magnitude of our coupling constant. Perhaps our approximations may need improvements to be realistic.

Hence we try to extrapolate our insights at high density into the lower-density domains, by arguing how correction terms grow up. Essentially interweaving chiral spirals are disturbed by the transverse dynamics and inter-patch interactions, and these effects become increasingly important at lower density. In this respect, we quote several elaborated numerical studies in the low-density side, in order to complement our current studies. At the same time, we will make use of our perturbative corrections to interpret some results in the existing literatures.

Related to our high density approximation, it is very important to know how the  $1/N_c$  corrections grow up at higher density. We will summarize effects which we have ignored by using the large- $N_c$  approximation.

Another important question is how our interweaving chiral spirals look like in coordinate space. Up to  $N_p = 3$ , the chiral density has a periodic translational order and an orientational order that are classified by usual crystallography. Beyond  $N_p = 3$ , however, the chiral density wave is no longer periodic, but just shows certain patterns with orientational symmetry. We briefly discuss these aspects, leaving several interesting questions open for future studies.

The remaining topic is the instanton-induced interaction [28], which is frequently used to introduce strong diquark correlations [29]. We will see that this interaction would provide quite different effects below and above the strange-quark threshold.

### 8.1 Comparisons with Other Works in the Low Density Regime

In Ref. [30], the authors have numerically studied the chiral crystals in (3+1) dimensions in the density region,  $\mu_q = 0.4-0.6$  GeV, using the NJL model and the model with the instanton-induced interactions. They studied the scalar-isoscalar channel with the plane-wave oscillations  $\sim \sigma e^{i\vec{Q}\cdot\vec{r}}$ . In the NJL model, the strength of the four-Fermi interaction becomes weaker at higher density because of the model cutoff, so they found only small mass gaps,  $\sim O(10)$  MeV. On the other hand, the instanton-induced interaction is stronger near the

Fermi surface, so it is possible to have a large mass gap of  $O(\Lambda_{\text{QCD}})$ . Importantly, they showed that the creation of the differently oriented chiral-density waves (crystals) does not provide much energy benefit, and the chiral density wave evolved only in one direction is energetically favored. This result can be interpreted as a consequence of inter-patch interactions, and is consistent with our current analysis.

In the case of the chiral density wave in one particular direction, there can be a better solution than the simple plane wave. Recently, such a solution in the (3+1)-dimensional NJL model was found by the authors of Ref. [15] who have used trial functionals motivated from (1+1)-dimensional studies [31]. The following results are deeply relevant to ours: (i) The solution appears to be of a solitonic type at low density, and approaches the plane-wave type at high density. (ii) A quark number modulation also occurs at low density. It smoothly approaches the uniform distribution as the density increases. (iii) The chiral spirals with  $\sigma$  and  $\vec{\pi}$ , which is naively expected, is not energetically favored as compared to single modulation of  $\sigma$ , as far as we keep  $\mu_u = \mu_d$ .

These statements are all consistent with our analyses, and in fact could be inferred from our framework as follows. Let us explain this in order.

(i) The deviation from the plane-wave solution is caused by the subdominant terms in our formulation,

$$\bar{\psi}'_+ \partial'_\perp \psi'_- e^{-2iQx_\parallel}, \quad (\bar{\psi}'_+ \psi'_-)^2 e^{-4iQx_\parallel}, \quad \dots \quad (100)$$

which provide higher harmonics necessary to construct solitonic solutions at low density<sup>18</sup>. As we discussed, these terms become unimportant as the density increases, recovering the plane-wave solutions.

(ii) In the computations of the expectation value of the quark number, the non-perturbative mean-field propagator gives uniform distribution, while the perturbations from subdominant terms can generate the spatial modulation (for more explanations, see Sec.8.3). The distribution approaches the uniform one as the density increases<sup>19</sup>.

<sup>18</sup> In (1+1) dimensions at  $T = 0$ , one can validate this discussion by investigating the Gross-Neveu (GN) model [32] with or without the continuous chiral symmetry. The former is free from the subdominant terms, and the chiral spirals can appear at arbitrary low density and the quark density is always uniform. (At nonzero  $T$ , we have the twisted kink crystal in which the amplitude field also modulates [33].) On the other hand, in the version with discrete chiral symmetry, solitonic objects first appear at density beyond some critical chemical potential which is slightly lower than the constituent quark mass. As density increases, subdominant terms stop to disturb the chiral rotation, then quark distributions smoothly approach those with the chiral spirals and uniform quark density. See also Sec. 6 in Ref. [6].

<sup>19</sup> Explicit calculations will be reported elsewhere.

(iii) It is quite straightforward to extend our one-flavor studies to the multi-flavor ones in terms of  $\Phi = (u, d, \dots)^T$ , and we can easily infer that the chiral spirals should emerge as a rotation in the  $U(1)$  quark number sector,

$$\langle \bar{\Phi}_+ \Phi_- \rangle = \Delta e^{-2iQx_{\parallel}}, \quad \langle \bar{\Phi}_- \Phi_+ \rangle = \Delta e^{2iQx_{\parallel}}, \quad (101)$$

which are equivalent with the following combination,

$$\langle \bar{\Phi} \Phi \rangle = 2\Delta \cos 2Qx_{\parallel}, \quad \langle \bar{\Phi} i\gamma_0 \gamma_{\parallel} \Phi \rangle = 2\Delta \sin 2Qx_{\parallel}. \quad (102)$$

The expectation value of the latter was not calculated in Ref. [15], though. Here we have not found any particular mechanism to generate flavor rotations, at least in the high-density limit. Of course, once we had explicit flavor breaking coming from conditions such as the charge neutrality and  $\beta$ -equilibrium<sup>20</sup>, they are likely to generate other chiral rotations as well. It would be interesting to consider astrophysical consequences of such inhomogeneous distributions. (See discussions on the implication to the glitch problem in Ref. [35], for example.)

Assembling these works and insights in this paper, let us infer what kind of calculations are desirable at low density. While the chiral crystals were not favored in the plane-wave Ansatz in Ref. [30], we know that higher harmonics become increasingly important at lower density, as shown in Ref. [15] and our perturbative calculations. They are relevant to describe a localized quark number density as well. An interesting question is whether crystals including higher harmonics are energetically more favored as compared to one-dimensional solitonic configuration in Ref. [15]. As discussed at the end of the previous section, inter-patch interactions are strong for the chiral spirals with close wavevectors. That argument, however, also implies that two chiral spirals with very different wavevectors do not strongly destroy one another. Thus, for configurations with higher harmonics, deconstruction due to inter-patch interactions might be tempered, so that the solitonic crystal structure might be energetically favored.

## 8.2 On the $1/N_c$ Corrections

As the density increases, the  $1/N_c$  corrections grow up because the increasing phase space around the Fermi surface enhances low-energy quark fluctuations<sup>21</sup>. The enhancement is parametrically  $\sim (\mu_q/\Lambda_{\text{QCD}})^{d-1}$  where  $d$  represents the number of spatial dimensions. Such effects are illustrated in the

<sup>20</sup> These conditions are driving mechanism to destabilize a homogeneous color-superconducting phases [34] into the crystalline states [35,36,37,38].

<sup>21</sup> Needless to say, when we try to include the  $1/N_c$  corrections, we have to restart all of the computations from the vacuum problem, in order to renormalize the theory

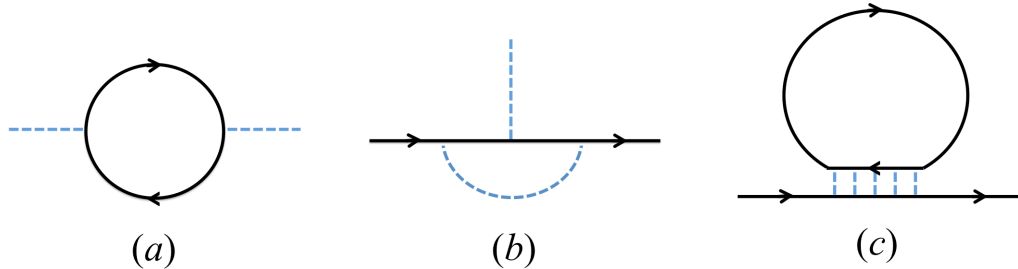


Fig. 17. Some diagrammatic examples of the  $1/N_c$  corrections for: (a) the gluon propagator, (b) the quark-gluon vertex, (c) our resummation scheme shown in the left panel in Fig. 4. Modifications by three- and four-gluon vertices should exist as well.

typical diagrams in Fig. 17. The diagrams (a) and (b) reduce the effective size of our coupling constant as the density increases. The diagram (c) modifies our resummation scheme or the mean-field treatment shown in Fig. 4. In the terminology of the four-Fermi interaction, we have treated the Hartree term while ignoring the Fock term in the large- $N_c$  limit, which will be modified.

Especially let us note that in the diagram (c), all momenta of the loop, the incoming quark, and the outgoing quark need not to be close, in contrast to the leading- $N_c$  contributions. Therefore once the  $1/N_c$  contributions to the condensate become comparable to the leading order, they will violate the locality of the quark-condensate interactions in momentum space. It means that inter-patch interactions among chiral spirals occur not only near the patch boundaries but everywhere near the Fermi surface. The situation becomes much more complicated than that we have treated in this paper.

The quantitative estimation of the  $1/N_c$  corrections is a highly non-linear problem. It should be quite sensitive to the effective masses of quarks, while the mass is determined by non-perturbative interactions whose strength is reduced by the screening effects by quarks. In this respect, it does matter whether we took into account possibilities of the inhomogeneous condensates or not. Under the assumption of homogeneous chiral symmetry breaking, quarks lose the mass gaps originated from quark-antiquark condensation, and then fluctuations would rapidly grow up at finite density. However, if we included a possibility of chiral symmetry breaking near the Fermi surface, the quarks acquire the mass gap through the constituent quark mass, suppressing the fluctuations near the Fermi surface. Calculations including the latter have not been done yet.

The above issue is also related to the validity of the stationary phase approximation. Here we have to distinguish two kinds of the fluctuations. One is

---

including fermion loops. Here we are arguing the medium-induced modification after the correct renormalization is made.

the amplitude fluctuation, largely related to the size of the quark mass gap. Another is the phase fluctuation, which is massless.

For the latter, one might suspect that, according to Mermin-Wagner-Coleman's arguments on lower dimensions [39], the IR fluctuations of the phases would be strong enough to destroy chiral spirals with quasi (1+1)-dimensional structure, and therefore quarks would lose their mass gaps.

A few remarks are in order. First, the absence of the spontaneous symmetry breaking in real (1+1) dimensions is extremely sensitive to the *deep* IR region. Our phase fluctuations cannot access such a region since the Fermi surface always has finite curvature effects which provide the IR cutoff<sup>22</sup>  $\sim p_{\perp}^2/p_F$ . So even without using the large- $N_c$  limit, we conclude that the chiral spirals have the long-range order. This issue was already addressed in Ref. [19].

Second, even if the system has only quasi long-range order, the mass gap is not washed out. The absence of the condensate does not mean the presence of a gapless quark, as far as the amplitude field takes a finite expectation value. For a (1+1)-dimensional example, see [43]. So a primary question concerned with the stationary phase approximation is whether the fields strongly fluctuate or not.

Besides the fluctuation effects, we should also mention on the possibility of the diquark condensate at  $N_c = 3$ , which could not be addressed in the large- $N_c$  limit. The Meissner effect would change our non-perturbative forces. This issue is beyond our scope, and can be addressed only by taking the energy competition between the interweaving chiral spirals and the color-superconducting phases.

### 8.3 A Coordinate Space Structure of the Interweaving Chiral Spirals

So far we have not discussed coordinate space structures of the interweaving chiral spirals. This is because like BCS theory, the energy minimization at high density is turned out to be sensitive only to the momentum space structures, at least in our model. This situation is very different from determination of crystal structures in atomic physics [40] where coordinate space descriptions are useful for the energy minimization.

Nevertheless, it is certainly interesting to illustrate how various densities in

---

<sup>22</sup> One might think that this cutoff argument would be inconsistent with our (1+1)-dimensional reduction of the gap equations. This is not so. The point is that the mass gap is much less sensitive to the *deep* infrared region — even if we omit such small phase space, we can find the solution, like the NJL model in vacuum.

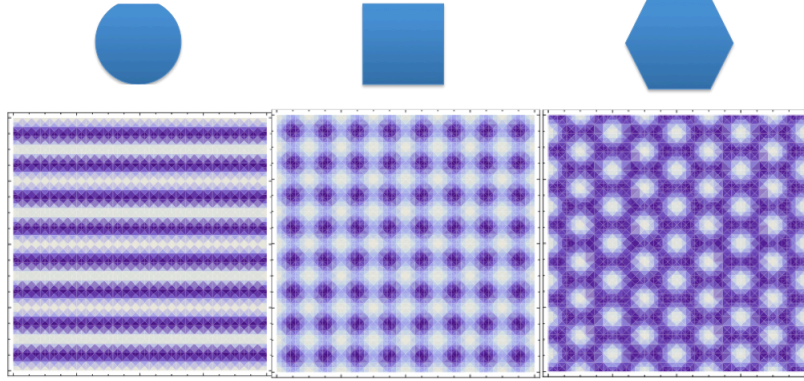


Fig. 18. The crystal structures of the chiral density for  $N_p = 1, 2, 3$ . The corresponding shapes of the Fermi sea are also shown. (For simplicity, we chose  $\vec{x}_i = \vec{0}$ .)

the interweaving chiral spirals look like in coordinate space. In practice, the coordinate space considerations have potential relevance for the considerations of the density domain close to baryonic matter, in which coordinate space descriptions of quarks are more appropriate than momentum space ones.

For a quark number density, the distribution is just uniform at the leading order of the high density expansion. This is because the quark number density made from different patch contributions,

$$\bar{\psi}\gamma_0\psi = \sum_{i=1}^{N_p} \left( \bar{\psi}_{i+}\gamma_0\psi_{i+} + \bar{\psi}_{i-}\gamma_0\psi_{i-} \right), \quad (103)$$

has no mixture of  $(+, -)$  fields. The spatially modulating contributions start to appear only after inclusion of perturbative corrections from subdominant terms such as  $\bar{\psi}_+ i \not{\partial}_\perp \psi_-$ , thus are suppressed at high density.

On the other hand, a distribution of the chiral density is nontrivial. After summing up contributions from different patches, we have

$$\langle \bar{\psi}\psi(x) \rangle = \sum_{i=1}^{N_p} \langle \bar{\psi}_{i+}\psi_{i-}(x) + \bar{\psi}_{i-}\psi_{i+}(x) \rangle \sim \Delta \sum_{i=1}^{N_p} \text{Re} \left( e^{2iQ\vec{n}_i \cdot (\vec{x} - \vec{x}_i)} \right), \quad (104)$$

where we did not write the form factor dependence for notational simplicity, and we took into account  $\vec{x}_i$  to make the amplitude field  $\Delta$  real.

Up to a patch number,  $N_p = 3$ , the chiral density has a periodic structure and an orientational symmetry known in the conventional crystallography. Shown in Fig. 18 are the crystal structures of chiral density, “chiral density crystals”, for  $N_p = 1, 2, 3$ .

The situation is, however, different beyond  $N_p = 3$ . The chiral density has only an  $Z_{2N_p}$  orientational symmetry, but does not possess a periodic structure (The

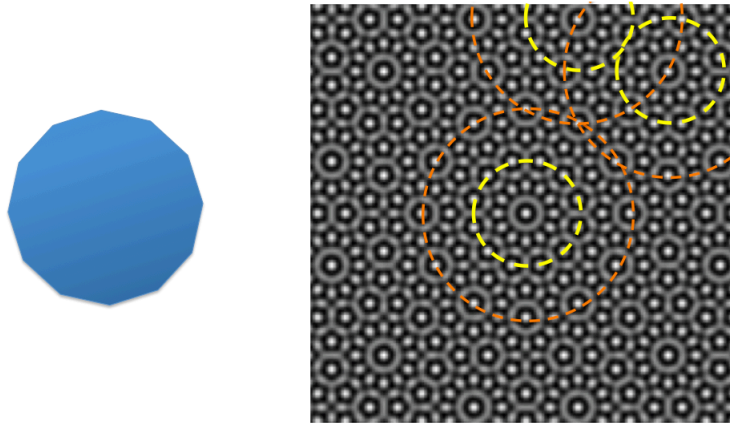


Fig. 19. The structures of the chiral density for  $N_p = 6$ . (Left) The shape of the Fermi sea. (Right) The coordinate space distributions of the chiral density where the center of figure is chosen as  $\vec{x} = \vec{0}$ . (For simplicity, we chose  $\vec{x}_i = \vec{0}$ .) Some circles connecting nodes are drawn as guidelines to look at patterns.

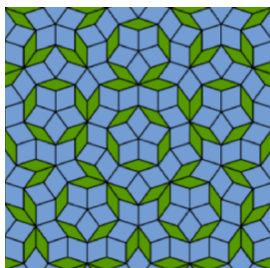


Fig. 20. The Penrose tiling as an example of two dimensional quasi-crystals. We have only two types of tiles to cover the entire space. There is no strict periodicity. (This figure is taken from Ref. [42].)

simple proof is given in Appendix C.) The spatial distributions show certain repeating patterns, though. (See Fig.19).

A natural question is whether interweaving chiral spirals with  $N_p \geq 4$  can be classified by structures known in the solid state physics. So far three types of solids have been known: (i) amorphous (or glassy) structures without any of the long-range correlations, (ii) crystal structures with periodic translational order and long-range (near-neighbor bond) orientational order with special crystallographic discrete subgroups of the rotational group, and (iii) quasi-crystal structures that can have arbitrary types of orientational symmetry and the corresponding quasi-periodicity [41]. A nontrivial fact is that in spite of lack of periodicity, quasi-crystals are made of a finite number of unit cell species. In Fig. 20 we show a specific example of two dimensional quasi-crystals which is known as Penrose tiling.

Interweaving chiral spirals state with  $N_p \geq 4$  does not have a periodicity,

so they are not crystals. Also, the interweaving chiral spirals have definite rotational properties and the size of wavevectors, so perhaps do not belong to amorphous.

It is not clear whether our interweaving chiral spirals belong to the remaining candidate, a quasi-crystal. In usual solids, their basic properties can be discussed by knowing ion species and their locations. The separation among ions are much larger than the size of ions, so it is good approximation to treat ion density as a sum of  $\delta$ -functions. The electron distribution is determined accordingly. Then we can attach a unit cell to each ion, and such cell structures appear repeatedly. Therefore studies of unit cells and their connections to other cells are enough to know properties of crystals. The relevant point here is that a number of cell and bond species is only finite.

In case of interweaving chiral spirals, it is tempting to assign nodes of interweaving chiral spirals as alternatives of positions of ions. The problem, however, is that unlike electron density in atomic crystals, the chiral density around nodes is not well-determined from locations of nodes, perhaps because the minimum energy configuration at high density is dominantly determined by momentum space structures. We expect that a number of varieties in cell shapes might be finite but contents in them might have a lot of varieties.

We leave further discussions about the classification of interweaving chiral spirals for future studies. We expect that such studies will become important for the region where the system changes from quark to baryonic matter, or appropriate descriptions for energy minimization changes from the momentum space to coordinate space one.

#### 8.4 On the Six-Fermi Interaction

Let us briefly mention on the effects of the six-Fermi interaction that breaks  $U(1)_A$  symmetry for three flavors. When we discuss dynamics of  $u, d$  quarks, we typically take the expectation value of  $\bar{s}s$ , and normalize the coupling constant as

$$\sim G_i (\bar{u}u)(\bar{d}d)(\bar{s}s) \longrightarrow \left(G_i \langle \bar{s}s \rangle\right) (\bar{u}u)(\bar{d}d) = G_i^s (\bar{u}u)(\bar{d}d), \quad (105)$$

where we did not write any explicit structure of the Dirac  $\gamma$  matrices. Thus at zero density, this interaction would renormalize the coupling constant of our model.

At high density, however, the four-Fermi and the six-Fermi interactions show interesting differences. Let us first consider the following situation;  $\mu \simeq \mu_u \simeq \mu_d \simeq \mu_s \gg \Lambda_{\text{QCD}}$ , where all light flavors form the quark Fermi sea. Using the



$\psi'_\pm$ -representation, the interaction looks like

$$\sim G_i \left( (\bar{u}'_+ u'_-) (\bar{d}'_+ d'_-) (\bar{s}'_+ s'_-) e^{-6i\mu_q x_\parallel} + (\bar{u}'_+ u'_-) (\bar{d}'_+ d'_-) (\bar{s}'_- s'_+) e^{-2i\mu_q x_\parallel} + \dots \right). \quad (106)$$

Here let us note that all of vertices must have oscillation factors, i.e., they are subdominant terms. These terms tend to disturb the chiral spiral formations, but eventually become negligible at very high density.

On the other hand, at intermediate density such that only  $u$  and  $d$  quarks have the Fermi sea, the vertex  $\langle \bar{s}' s' \rangle$  is uniform and does not include the oscillating factor. Then we can find the dominant four-Fermi interactions which help the formation of the chiral spirals in the  $u, d$  channels. Actually this is the situation discussed in the aforementioned work [30]. It is interesting to see whether any drastic changes happen near the strange-quark threshold.

## 9 Summary

In this paper we have argued how to construct the interweaving chiral spirals at high density. The patch size is determined by the balance between the energy gain from condensation and the energy cost from the deformed Fermi surface. The Fermi surface effects drove the spontaneous breaking of chiral, translational, and rotational invariance.

A key ingredient of our discussions was that the interaction among quarks and the condensate, which is dominant at large  $N_c$ , was local in momentum space. Because of this property, energy contributions could be characterized by the limited phase space for the scattering between quarks and the condensate. In particular, complicated interplay between differently oriented chiral spirals happen only near the patch boundaries, so we could roughly estimate the energy cost by just seeing the phase space for patch-patch interactions.

We have argued the (2+1)-dimensional model for which the geometric shape of the Fermi sea is relatively simple. In reality with higher dimensions, however, such simplicity is no longer the case since there are many ways to interweave chiral spirals. On the other hand, the principle to choose the best shape should be relatively simple according to the arguments in this paper. We need get the largest energy gain from condensation by maximizing the area of the Fermi surface until the kinetic energy cost becomes crucial, and at the same time, we have to minimize the length of the patch intersection lines to reduce inter-patch interactions. To find such a geometric shape would be a mathematically well-defined problem.

The interweaving chiral spirals will survive in (3+1) dimensions, since the key point is the IR enhancement of the interaction, which is the fundamental property based on QCD. This situation is quite different from charge or spin density waves in condensed matter physics, which are energetically favored in one-dimensional systems, but not in higher dimensions [44].

The form of the chiral Lagrangian near the Fermi surface was derived in Ref. [19], regarding the system near the Fermi surface as the (1+1)-dimensional chains with the transverse hopping. In the dispersion relation for the collective modes, transverse kinetic terms are suppressed by powers of  $\Lambda_f/Q$ . As the density increases, therefore, the spectrum will approach the (1+1)-dimensional one, so that the IR fluctuations will be stronger. We also anticipate that the temperature effects strongly enhance the phase fluctuations [45]. Results on this issue will be reported in the future.

## Acknowledgments

We thank G. Basar, G. Dunne, E.J. Ferrer, L.Y. Glozman, V. Incera, J. Liao, S. Nakamura, R. Rapp, E. Shuryak, G. Torrieri, and I. Zahed for useful comments and/or raising several important questions related to multiple (Quarkyonic) chiral spirals. Special thanks go to A.M. Tsvetik for the collaboration [19] with several of the present authors. We acknowledge the referee for constructive questions which have helped us to improve the original manuscript. T.K. acknowledges to S. Carignano and M. Buballa for explaining their NJL model studies on the chiral crystals before the publication. He also thanks the Asia Pacific Center for Theoretical Physics (APCTP) and Hashimoto Laboratory in RIKEN Nishina Center for their hospitality during his visit in March and April 2011. The research of Y.H. is supported by RIKEN and the Grand-in-Aid for the Global COE Program “The Next Generation of Physics, Spun from Universality and Emergence” from the Ministry of Education, Culture, Science and Technology (MEXT) of Japan; that of T.K. by the Postdoctoral Research Program of RIKEN; that of L.D.M. and R.D.P. by the U.S. Department of Energy under contract No. DE-AC02-98CH10886. R.D.P. also thanks the Alexander von Humboldt Foundation for their support.

## A The single particle dispersion for $\vec{q} \neq 2Q\vec{n}$

In this work we have assumed  $\vec{q} = 2Q\vec{n}$  in the (1+1) dimensional construction. Here we show what will happen if we chose a different wavevector. To do this,

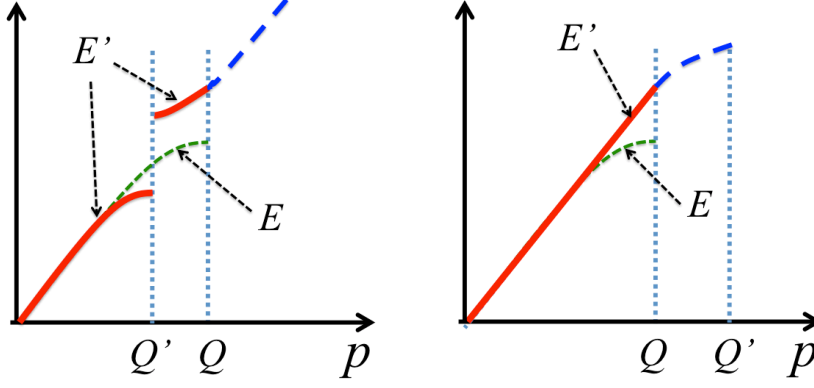


Fig. A.1. The single particle dispersion  $E'$  for  $Q' < Q$  (left) and  $Q' > Q$  (right) cases. Because of the particle number constraint, particles must occupy up to  $p = Q$ . The  $Q' = Q$  case with the energy  $E$  is also plotted as a guideline.

we go back to the original  $\psi$  bases, and write the eigenvalue equation,

$$\Psi^\dagger \begin{pmatrix} i\partial_{\parallel} & Me^{2iQ'x_{\parallel}} \\ Me^{-2iQ'x_{\parallel}} & -i\partial_{\parallel} \end{pmatrix} \Psi(x_{\parallel}) = E'_{\text{MF}} (\Psi^\dagger \Psi(x_{\parallel})), \quad (\text{A.1})$$

where we omit the form factor effects on  $M$  for the sake of simplicity. To diagonalize it, we choose  $\psi_{\pm} = \psi''_{\pm} e^{\pm iQ'x_{\parallel}}$ , and eliminate the oscillating factors. The energy for the right moving branch is

$$E'_{\text{MF}}(p_{\parallel}) = Q' \pm \sqrt{(p_{\parallel} - Q')^2 + M^2}, \quad (\text{A.2})$$

and its behavior for  $Q' < Q$  and  $Q' > Q$  is shown in Fig. A.1 with the guideline of the  $Q' = Q$  case. With the particle number constraint, we have to put particles up to the momentum  $Q$ . For  $Q' < Q$ , the particles occupy the upper branch, costing energy. For  $Q' > Q$ , the particles occupy only the lower branch, but the energetic benefit is small because of the distance from the gap region. Therefore the case of  $Q' = Q$  is the best way to minimize the total single particle contributions. If we add the corrections to the (1+1) dimensional approximations, it can deviate from  $Q' = Q$ , though.

## B A component expression of the mean field propagator

In the computation of the perturbative corrections, it is useful to use the component expressions which are decomposed into different pole structures. Explicitly, ( $\omega = \omega(\delta\vec{p})$ )

$$\begin{aligned}
S_{++}(\delta p) &= i \times \frac{1 + \Gamma_5}{2} \times \frac{\gamma^0}{2} \left[ \frac{1 + \delta p_{\parallel}/\omega}{\delta p_0 - \omega + i\epsilon} + \frac{1 - \delta p_{\parallel}/\omega}{\delta p_0 + \omega - i\epsilon} \right], \\
S_{--}(\delta p) &= i \times \frac{1 - \Gamma_5}{2} \times \frac{\gamma^0}{2} \left[ \frac{1 - \delta p_{\parallel}/\omega}{\delta p_0 - \omega + i\epsilon} + \frac{1 + \delta p_{\parallel}/\omega}{\delta p_0 + \omega - i\epsilon} \right], \quad (\text{B.1})
\end{aligned}$$

and

$$S_{+-}(\delta p) = \frac{1 + \Gamma_5}{2} S_M, \quad S_{-+}(\delta p) = \frac{1 - \Gamma_5}{2} S_M, \quad (\text{B.2})$$

where

$$S_M(\delta p) = i \times \frac{M}{2\omega} \left[ \frac{1}{\delta p_0 - \omega + i\epsilon} - \frac{1}{\delta p_0 + \omega - i\epsilon} \right]. \quad (\text{B.3})$$

### C There is no periodic structure for $N_p \geq 4$

We shall explain why interweaving chiral spirals with  $N_p \geq 4$  can not have a periodic structure. For simplicity, we will consider only wavevectors in differently oriented chiral spirals have common  $Q$ .

Suppose that the condensate is invariant under the translation,  $\vec{x} \rightarrow \vec{x} - \vec{a}$ ,

$$\langle \bar{\psi} \psi(\vec{x}) \rangle = \langle \bar{\psi} \psi(\vec{x} + \vec{a}) \rangle = \Delta \sum_{i=0}^{N_p-1} \text{Re} \left( e^{2iQ\vec{n}_i \cdot \vec{a}} e^{2iQ\vec{n}_i \cdot (\vec{x} - \vec{x}_i)} \right). \quad (\text{C.1})$$

To satisfy this equation for arbitrary  $\vec{x}$ , the condition

$$2Q \vec{n}_i \cdot \vec{a} = 2\pi m_i, \quad (m_i : \text{integer}) \quad (\text{C.2})$$

must be satisfied for all  $i$ .

We choose  $(x, y)$  axis in such a way that  $\vec{n}_k$  is expressed as

$$\vec{n}_k = \left( \cos \left( \frac{\pi k}{N_p} \right), \sin \left( \frac{\pi k}{N_p} \right) \right), \quad (k = 0, 1, \dots, N_p - 1) \quad (\text{C.3})$$

And we take  $\vec{a}$  as

$$\vec{a} = a (\cos \varphi, \sin \varphi). \quad (\text{C.4})$$

Then the condition (C.2) is

$$2Qa \cos \left( \varphi - \frac{\pi k}{N_p} \right) = 2\pi m_k. \quad (m_k : \text{integer}) \quad (\text{C.5})$$

This condition should be satisfied for all  $k$ . We wish to know whether we can choose  $a$  and  $\varphi$  to satisfy this condition.

The ratio

$$\frac{\cos\left(\varphi - \frac{\pi k}{N_p}\right)}{\cos\varphi} = \cos\left(\frac{\pi k}{N_p}\right) + \tan\varphi \sin\left(\frac{\pi k}{N_p}\right) = \frac{m_k}{m_0}, \quad (\text{C.6})$$

must be rational number. If we also consider  $N_p - k$  case, we obtain

$$\frac{\cos\left(\varphi - \frac{\pi(N_p - k)}{N_p}\right)}{\cos\varphi} = -\cos\left(\frac{\pi k}{N_p}\right) + \tan\varphi \sin\left(\frac{\pi k}{N_p}\right) = \frac{m_{N_p - k}}{m_0}. \quad (\text{C.7})$$

After subtraction, we have

$$2 \cos\left(\frac{\pi k}{N_p}\right) = \frac{m_k - m_{N_p - k}}{m_0}. \quad (\text{C.8})$$

Therefore the LHS must be rational number for all  $k$ . This is necessary condition. For  $N_p \geq 4$ ,  $\cos(\pi k/N_p)$  has an irrational number, and the periodic condition is not satisfied.

## References

- [1] L. McLerran, R. D. Pisarski, Nucl. Phys. A **796** (2007) 83 [arXiv:0706.2191 [hep-ph]].
- [2] Y. Hidaka, L. D. McLerran, R. D. Pisarski, Nucl. Phys. A **808** (2008) 117 [arXiv:0803.0279 [hep-ph]].
- [3] L. Y. Glozman, R. F. Wagenbrunn, Phys. Rev. D **77** (2008) 054027 [arXiv:0709.3080 [hep-ph]]; L. Y. Glozman, Phys. Rev. **D79** (2009) 037504 [arXiv:0812.1101 [hep-ph]]; L. McLerran, K. Redlich, C. Sasaki, Nucl. Phys. A **824** (2009) 86 [arXiv:0812.3585 [hep-ph]]; K. Miura, T. Z. Nakano, A. Ohnishi, Prog. Theor. Phys. **122** (2009) 1045 [arXiv:0806.3357 [nucl-th]]; S. Hands, S. Kim, J. -I. Skullerud, Phys. Rev. **D81** (2010) 091502 [arXiv:1001.1682 [hep-lat]].
- [4] K. Fukushima, Phys. Rev. **D77** (2008) 114028 [arXiv:0803.3318 [hep-ph]]; J. Phys. G **G35** (2008) 104020 [arXiv:0806.0292 [hep-ph]]; K. Fukushima, T. Hatsuda, Rept. Prog. Phys. **74** (2011) 014001 [arXiv:1005.4814 [hep-ph]].
- [5] A. Andronic *et al.*, Nucl. Phys. A **837** (2010) 65 [arXiv:0911.4806 [hep-ph]].
- [6] T. Kojo, arXiv:1106.2187 [hep-ph].
- [7] G. 't Hooft, Nucl. Phys. B **72** (1974) 461; Nucl. Phys. B **75** (1974) 461; E. Witten, Nucl. Phys. B **160** (1979) 57.

- [8] O. Kaczmarek *et al.*, Phys. Rev. **D83** (2011) 014504 [arXiv:1011.3130 [hep-lat]]; G. Endrodi, Z. Fodor, S. D. Katz, K. K. Szabo, JHEP **1104** (2011) 001 [arXiv:1102.1356 [hep-lat]].
- [9] B. -J. Schaefer, J. M. Pawłowski, J. Wambach, Phys. Rev. **D76** (2007) 074023 [arXiv:0704.3234 [hep-ph]]; T. K. Herbst, J. M. Pawłowski and B. J. Schaefer, Phys. Lett. B **696** (2011) 58 [arXiv:1008.0081 [hep-ph]]; K. Fukushima, Phys. Lett. **B695** (2011) 387 [arXiv:1006.2596 [hep-ph]].
- [10] A. Casher, Phys. Lett. B **83** (1979) 395; T. Banks, A. Casher, Nucl. Phys. B **169** (1980) 103.
- [11] D. V. Deryagin, D. Y. Grigoriev, V. A. Rubakov, Int. J. Mod. Phys. A **7** (1992) 659.
- [12] E. Shuster, D. T. Son, Nucl. Phys. B **573** (2000) 434 [hep-ph/9905448].
- [13] B. Y. Park, M. Rho, A. Wirzba, I. Zahed, Phys. Rev. D **62** (2000) 034015 [hep-ph/9910347].
- [14] M. Sadzikowski, W. Broniowski, Phys. Lett. B **488** (2000) 63 [arXiv:hep-ph/0003282]; E. Nakano, T. Tatsumi, Phys. Rev. D **71** (2005) 114006 [arXiv:hep-ph/0411350]; B. Bringoltz, JHEP **0703** (2007) 016 [arXiv:hep-lat/0612010]; M. Sadzikowski, Phys. Lett. B **553** (2003) 45 [arXiv:hep-ph/0210065]; Phys. Lett. B **642** (2006) 238 [arXiv:hep-ph/0609186]; T. L. Partyka and M. Sadzikowski, J. Phys. G **36** (2009) 025004 [arXiv:0811.4616 [hep-ph]]; Acta Phys. Polon. B **42** (2011) 1305 [arXiv:1011.0921 [hep-ph]];
- [15] D. Nickel, Phys. Rev. Lett. **103** (2009) 072301 [arXiv:0902.1778 [hep-ph]]; Phys. Rev. D **80** (2009) 074025 [arXiv:0906.5295 [hep-ph]]; S. Carignano, D. Nickel, M. Buballa, Phys. Rev. D **82** (2010) 054009 [arXiv:1007.1397 [hep-ph]].
- [16] A. B. Migdal, Rev. Mod. Phys. **50** (1978) 107-172.
- [17] T. Kojo, Y. Hidaka, L. McLerran, R. D. Pisarski, Nucl. Phys. A **843** (2010) 37 [arXiv:0912.3800 [hep-ph]].
- [18] R. Casalbuoni, R. Gatto, M. Mannarelli, G. Nardulli, Phys. Lett. B **511** (2001) 218 [arXiv:hep-ph/0101326].
- [19] T. Kojo, R. D. Pisarski, A. M. Tsvelik, Phys. Rev. D **82** (2010) 074015 [arXiv:1007.0248 [hep-ph]].
- [20] Y. Nambu, G. Jona-Lasinio, Phys. Rev. **122** (1961) 345; Phys. Rev. **124** (1961) 246.
- [21] For reviews, see; U. Vogl, W. Weise, Prog. Part. Nucl. Phys. **27** (1991) 195; S. P. Klevansky, Rev. Mod. Phys. **64** (1992) 649; T. Hatsuda, T. Kunihiro, Phys. Rept. **247** (1994) 221 [arXiv:hep-ph/9401310]; M. Buballa, Phys. Rept. **407** (2005) 205 [arXiv:hep-ph/0402234].

- [22] L. Y. Glozman, Phys. Lett. B **475** (2000) 329 [arXiv:hep-ph/9908207]; Phys. Lett. B **541** (2002) 115 [arXiv:hep-ph/0204006]; Phys. Lett. B **539** (2002) 257 [arXiv:hep-ph/0205072]; Phys. Rept. **444** (2007) 1 [arXiv:hep-ph/0701081]; Phys. Rev. Lett. **99** (2007) 191602 [arXiv:0706.3288 [hep-ph]]; T. D. Cohen, L. Y. Glozman, Phys. Rev. D **65** (2001) 016006 [arXiv:hep-ph/0102206]; Int. J. Mod. Phys. A **17** (2002) 1327 [arXiv:hep-ph/0201242]; L. Y. Glozman and A. V. Nefediev, Phys. Rev. D **73** (2006) 074018 [arXiv:hep-ph/0603025]; Phys. Rev. D **76** (2007) 096004 [arXiv:0704.2673 [hep-ph]]; Nucl. Phys. A **807**, 38 (2008) [arXiv:0801.4343 [hep-ph]]; R. F. Wagenbrunn and L. Y. Glozman, Phys. Lett. B **643** (2006) 98 [arXiv:hep-ph/0605247]; Phys. Rev. D **75** (2007) 036007 [arXiv:hep-ph/0701039].
- [23] M. Shifman, A. Vainshtein, Phys. Rev. D **77** (2008) 034002 [arXiv:0710.0863 [hep-ph]].
- [24] M. Buballa, S. Krewald, Phys. Lett. B **294** (1992) 19; R. D. Bowler, M. C. Birse, Nucl. Phys. A **582** (1995) 655 [arXiv:hep-ph/9407336]; R. S. Plant, M. C. Birse, Nucl. Phys. A **628** (1998) 607 [arXiv:hep-ph/9705372]; A. H. Rezaeian, N. R. Walet, M. C. Birse, Phys. Rev. C **70** (2004) 065203 [arXiv:hep-ph/0408233]; I. General, D. Gomez Dumm, N. N. Scoccola, Phys. Lett. B **506** (2001) 267 [arXiv:hep-ph/0010034]; D. Gomez Dumm, N. N. Scoccola, Phys. Rev. D **65** (2002) 074021 [arXiv:hep-ph/0107251]; Phys. Rev. C **72** (2005) 014909 [arXiv:hep-ph/0410262]; A. Scarpettini, D. Gomez Dumm, N. N. Scoccola, Phys. Rev. D **69** (2004) 114018 [arXiv:hep-ph/0311030]; D. Gomez Dumm, D. B. Blaschke, A. G. Grunfeld, N. N. Scoccola, Phys. Rev. D **73** (2006) 114019 [arXiv:hep-ph/0512218]; W. Broniowski, B. Golli, G. Ripka, Nucl. Phys. A **703** (2002) 667 [arXiv:hep-ph/0107139]; A. H. Rezaeian, H. J. Pirner, Nucl. Phys. A **769** (2006) 35 [arXiv:nucl-th/0510041]; A. E. Radzhabov, D. Blaschke, M. Buballa, M. K. Volkov, Phys. Rev. D **83** (2011) 116004 [arXiv:1012.0664 [hep-ph]]; T. Hell, S. Rossner, M. Cristoforetti, W. Weise, Phys. Rev. D **81** (2010) 074034 [arXiv:0911.3510 [hep-ph]]; T. Hell, K. Kashiwa, W. Weise, arXiv:1104.0572 [hep-ph].
- [25] V. N. Gribov, Nucl. Phys. B **139** (1978) 1; A. Szczepaniak, E. S. Swanson, C. R. Ji, S. R. Cotanch, Phys. Rev. Lett. **76** (1996) 2011 [arXiv:hep-ph/9511422]; A. P. Szczepaniak, E. S. Swanson, Phys. Rev. D **65** (2002) 025012 [arXiv:hep-ph/0107078]; D. Zwanziger, Nucl. Phys. B **518** (1998) 237; Phys. Rev. Lett. **90** (2003) 102001 [arXiv:hep-lat/0209105]; J. Greensite, S. Olejnik, D. Zwanziger, Phys. Rev. D **69** (2004) 074506 [arXiv:hep-lat/0401003]; JHEP **0505** (2005) 070 [arXiv:hep-lat/0407032]; C. S. Fischer, D. Zwanziger, Phys. Rev. D **72** (2005) 054005 [arXiv:hep-ph/0504244].
- [26] D. K. Hong, Phys. Lett. **B473** (2000) 118 [hep-ph/9812510]; Nucl. Phys. **B582** (2000) 451 [hep-ph/9905523]; D. K. Hong, S. D. H. Hsu, Phys. Rev. **D66** (2002) 071501 [hep-ph/0202236].
- [27] T. W. Appelquist, M. J. Bowick, D. Karabali, L. C. R. Wijewardhana, Phys. Rev. **D33** (1986) 3704.
- [28] M. Kobayashi and T. Maskawa, Prog. Theor. Phys. **44**, 1422 (1970); M. Kobayashi, H. Kondo and T. Maskawa, Prog. Theor. Phys. **45**, 1955 (1971);

- G. 't Hooft, Phys. Rev. Lett. **37** (1976) 8; Phys. Rev. D **14** (1976) 3432 [Erratum-ibid. D **18** (1978) 2199].
- [29] R. Rapp, T. Schafer, E. V. Shuryak, M. Velkovsky, Phys. Rev. Lett. **81** (1998) 53 [arXiv:hep-ph/9711396]; Annals Phys. **280** (2000) 35 [arXiv:hep-ph/9904353]; M. G. Alford, K. Rajagopal, F. Wilczek, Phys. Lett. B **422** (1998) 247 [arXiv:hep-ph/9711395].
- [30] R. Rapp, E. V. Shuryak, I. Zahed, Phys. Rev. D **63** (2001) 034008 [arXiv:hep-ph/0008207].
- [31] V. Schon, M. Thies, arXiv:hep-th/0008175; O. Schnetz, M. Thies, K. Urlichs, Annals Phys. **314** (2004) 425 [arXiv:hep-th/0402014]; Annals Phys. **321** (2006) 2604 [arXiv:hep-th/0511206]; M. Thies, J. Phys. A **39** (2006) 12707 [arXiv:hep-th/0601049]; C. Boehmer, M. Thies, Phys. Rev. D **80** (2009) 125038 [arXiv:0909.3714 [hep-th]].
- [32] D. J. Gross, A. Neveu, Phys. Rev. D **10**, 3235 (1974).
- [33] G. Basar and G. V. Dunne, Phys. Rev. Lett. **100** (2008) 200404 [arXiv:0803.1501 [hep-th]]; Phys. Rev. D **78** (2008) 065022 [arXiv:0806.2659 [hep-th]]; JHEP **1101** (2011) 127 [arXiv:1011.3835 [hep-th]]; G. Basar, G. V. Dunne, M. Thies, Phys. Rev. D **79** (2009) 105012 [arXiv:0903.1868 [hep-th]].
- [34] M. Huang, I. A. Shovkovy, Phys. Rev. **D70** (2004) 051501 [hep-ph/0407049]; Phys. Rev. **D70** (2004) 094030 [hep-ph/0408268]; R. Casalbuoni, R. Gatto, M. Mannarelli, G. Nardulli, M. Ruggieri, Phys. Lett. **B605** (2005) 362 [hep-ph/0410401]; K. Fukushima, Phys. Rev. **D72** (2005) 074002 [hep-ph/0506080]; [hep-ph/0510299]; Phys. Rev. D **73** (2006) 094016 [arXiv:hep-ph/0603216]; I. Giannakis, J. T. Liu, H. C. Ren, Phys. Rev. D **66** (2002) 031501 [arXiv:hep-ph/0202138]; I. Giannakis, H. C. Ren, Phys. Lett. B **611** (2005) 137 [arXiv:hep-ph/0412015]; Nucl. Phys. B **723** (2005) 255 [arXiv:hep-th/0504053]; I. Giannakis, D. F. Hou, H. C. Ren, Phys. Lett. B **631** (2005) 16 [arXiv:hep-ph/0507306]; I. Giannakis, D. Hou, M. Huang, H. C. Ren, Phys. Rev. D **75** (2007) 014015 [arXiv:hep-ph/0609098].
- [35] M. G. Alford, J. A. Bowers, K. Rajagopal, Phys. Rev. D **63** (2001) 074016 [arXiv:hep-ph/0008208]; J. A. Bowers, J. Kundu, K. Rajagopal, E. Shuster, Phys. Rev. D **64** (2001) 014024 [arXiv:hep-ph/0101067]; A. K. Leibovich, K. Rajagopal, E. Shuster, Phys. Rev. D **64** (2001) 094005 [arXiv:hep-ph/0104073]; J. Kundu, K. Rajagopal, Phys. Rev. D **65** (2002) 094022 [arXiv:hep-ph/0112206]; J. A. Bowers, K. Rajagopal, Phys. Rev. D **66** (2002) 065002 [arXiv:hep-ph/0204079]; K. Rajagopal, R. Sharma, Phys. Rev. D **74** (2006) 094019 [arXiv:hep-ph/0605316]; M. Mannarelli, K. Rajagopal, R. Sharma, Phys. Rev. D **76** (2007) 074026 [arXiv:hep-ph/0702021].
- [36] R. Casalbuoni, R. Gatto, M. Mannarelli, G. Nardulli, Phys. Rev. D **66** (2002) 014006 [arXiv:hep-ph/0201059]; R. Casalbuoni, R. Gatto, G. Nardulli, Phys. Lett. B **543** (2002) 139 [arXiv:hep-ph/0205219]; R. Casalbuoni, E. Fabiano, R. Gatto, M. Mannarelli, G. Nardulli, Phys. Rev. D **66** (2002) 094006



- [arXiv:hep-ph/0208121]; R. Casalbuoni, G. Nardulli, Rev. Mod. Phys. **76** (2004) 263 [arXiv:hep-ph/0305069]; R. Casalbuoni, M. Ciminale, M. Mannarelli, G. Nardulli, M. Ruggieri, R. Gatto, Phys. Rev. D **70** (2004) 054004 [arXiv:hep-ph/0404090]; R. Casalbuoni, R. Gatto, N. Ippolito, G. Nardulli, M. Ruggieri, Phys. Lett. B **627** (2005) 89 [Erratum-ibid. B **634** (2006) 565] [arXiv:hep-ph/0507247]; M. Ciminale, G. Nardulli, M. Ruggieri, R. Gatto, Phys. Lett. B **636** (2006) 317 [arXiv:hep-ph/0602180]; R. Casalbuoni, M. Ciminale, R. Gatto, G. Nardulli, M. Ruggieri, Phys. Lett. B **642** (2006) 350 [arXiv:hep-ph/0606242]; R. Anglani, G. Nardulli, M. Ruggieri, M. Mannarelli, Phys. Rev. D **74** (2006) 074005 [arXiv:hep-ph/0607341].
- [37] O. Kiriya, D. H. Rischke, I. A. Shovkovy, Phys. Lett. B **643** (2006) 331 [arXiv:hep-ph/0606030]; N. Ippolito, M. Ruggieri, D. Rischke, A. Sedrakian, F. Weber, Phys. Rev. D **77** (2008) 023004 [arXiv:0710.3874 [astro-ph]]; A. Sedrakian, D. H. Rischke, Phys. Rev. D **80** (2009) 074022 [arXiv:0907.1260 [nucl-th]].
- [38] E. V. Gorbar, M. Hashimoto, V. A. Miransky, Phys. Rev. Lett. **96** (2006) 022005 [arXiv:hep-ph/0509334]; K. Fukushima, K. Iida, Phys. Rev. D **76** (2007) 054004 [arXiv:0705.0792 [hep-ph]]; L. M. Lin, Phys. Rev. D **76** (2007) 081502 [arXiv:0708.2965 [astro-ph]]; T. Brauner, Phys. Rev. D **78** (2008) 125027 [arXiv:0810.3481 [hep-ph]]; D. Nickel, M. Buballa, Phys. Rev. D **79** (2009) 054009 [arXiv:0811.2400 [hep-ph]].
- [39] N. D. Mermin and H. Wagner, Phys. Rev. Lett. **17** (1966) 1133; S. R. Coleman, Commun. Math. Phys. **31** (1973) 259.
- [40] N.W. Ashcroft and N.D. Mermin, *Solid State Physics*, Thomson Learning (1976); L.D. Landau and E.M. Lifshitz, *Statistical Physics*, Butterworth-Heinemann (1980).
- [41] D. Shechtman, I. Blech, D. Gratias, and J.W. Cahn, Phys. Rev. Lett. **53**, 1951 (1984); D. Levine and P. J. Steinhardt, Phys. Rev. Lett. **53**, 2477 (1984); J.E.S. Socolar, P.J. Steinhardt, and D. Levine, Phys. Rev. B **32**, 5547 (1985); D. Levine and P.J. Steinhardt, Phys. Rev. B **34**, 596 (1986); J.E.S. Socolar and P.J. Steinhardt, Phys. Rev. B **34**, 617 (1986).
- [42] [http://en.wikipedia.org/wiki/File:Penrose\\_Tiling\\_\(Rhombi\).svg](http://en.wikipedia.org/wiki/File:Penrose_Tiling_(Rhombi).svg).
- [43] E. Witten, Nucl. Phys. B **145** (1978) 110.
- [44] E. Dagotto, Rev. Mod. Phys. **66** (1994) 763.
- [45] G. Baym, B. L. Friman and G. Grinstein, Nucl. Phys. B **210** (1982) 193.